NAVAL POSTGRADUATE SCHOOL

MONTEREY, CALIFORNIA

THESIS

A PULSED POWER SYSTEM DESIGN USING LITHIUM-ION BATTERIES AND ONE CHARGER PER BATTERY

by

Frank E. Filler

December 2009

Thesis Advisor:	Alexander L. Julian
Second Reader:	Roberto Cristi

REPORT DOCUMENTATION PAGE		*Form Approved OMB No. 0704-0188*
Public reporting burden for this collection of information is estimated to average 1 hour per response, including the time for reviewing instruction, searching existing data sources, gathering and maintaining the data needed, and completing and reviewing the collection of information. Send comments regarding this burden estimate or any other aspect of this collection of information, including suggestions for reducing this burden, to Washington headquarters Services, Directorate for Information Operations and Reports, 1215 Jefferson Davis Highway, Suite 1204, Arlington, VA 22202-4302, and to the Office of Management and Budget, Paperwork Reduction Project (0704-0188) Washington DC 20503.		
1. AGENCY USE ONLY *(Leave blank)*	**2. REPORT DATE** December 2009	**3. REPORT TYPE AND DATES COVERED** Master's Thesis
4. TITLE AND SUBTITLE A Pulsed Power System Design Using Lithium-ion Batteries and One Charger per Battery		**5. FUNDING NUMBERS**
6. AUTHOR(S) Frank E. Filler		
7. PERFORMING ORGANIZATION NAME(S) AND ADDRESS(ES) Naval Postgraduate School Monterey, CA 93943-5000		**8. PERFORMING ORGANIZATION REPORT NUMBER**
9. SPONSORING /MONITORING AGENCY NAME(S) AND ADDRESS(ES) N/A		**10. SPONSORING/MONITORING AGENCY REPORT NUMBER**
11. SUPPLEMENTARY NOTES The views expressed in this thesis are those of the author and do not reflect the official policy or position of the Department of Defense or the U.S. Government.		
12a. DISTRIBUTION / AVAILABILITY STATEMENT Approved for public release; distribution is unlimited		**12b. DISTRIBUTION CODE** A
13. ABSTRACT (maximum 200 words) The work documented in this thesis realizes a small-scale implementation of a Battery Management System (BMS) that has the charging, storage, and discharge capabilities to meet scaled down requirements of a pulsed power system. Further, this work establishes a flexible battery research and testing capability resident at the Naval Postgraduate School (NPS). The designed architecture will provide this flexibility by providing the capability to change charging methodologies and types of batteries with only a change of the FPGA software. The BMS design uses lithium-ion batteries as the energy storage medium and uses one charger per battery for maximum charging flexibility. In order to meet a pulsed power system's requirements, the BMS performs three functions: charging lithium-ion batteries, storing energy for the pulsed power application in lithium-ion batteries, and discharging the energy in pulses to simulate the requirements of a pulse power system. To perform these three functions the BMS has several elements to include the power source, the charger, the batteries, the FPGA controller, and the discharge mechanism. The design and construction of the BMS and these individual elements are explored in detail in this thesis.		
14. SUBJECT TERMS Pulsed Power, Charger, Buck Converter, Field Programmable Gate Array (FPGA), Lithium-ion Batteries		**15. NUMBER OF PAGES** 102
		16. PRICE CODE
17. SECURITY CLASSIFICATION OF REPORT Unclassified	**18. SECURITY CLASSIFICATION OF THIS PAGE** Unclassified	**19. SECURITY CLASSIFICATION OF ABSTRACT** Unclassified	**20. LIMITATION OF ABSTRACT** UU

THIS PAGE INTENTIONALLY LEFT BLANK

A PULSED POWER SYSTEM DESIGN USING LITHIUM-ION BATTERIES AND ONE CHARGER PER BATTERY

Frank E. Filler
Major, United States Marine Corps
B.S., United States Naval Academy, 1997

Submitted in partial fulfillment of the
requirements for the degree of

MASTER OF SCIENCE IN ELECTRICAL ENGINEERING

from the

**NAVAL POSTGRADUATE SCHOOL
December 2009**

Author: Frank E. Filler

Approved by: Alexander L. Julian
Thesis Advisor

Roberto Crisiti
Second Reader

Jeffrey B. Knorr
Chairman, Department of Electrical and
Computer Engineering

THIS PAGE INTENTIONALLY LEFT BLANK

ABSTRACT

The work documented in this thesis realizes a small-scale implementation of a Battery Management System (BMS) that has the charging, storage, and discharge capabilities to meet scaled down requirements of a pulsed power system. Further, this work establishes a flexible battery research and testing capability resident at the Naval Postgraduate School (NPS). The designed architecture will provide this flexibility by providing the capability to change charging methodologies and types of batteries with only a change of the FPGA software. The BMS design uses lithium-ion batteries as the energy storage medium and uses one charger per battery for maximum charging flexibility. In order to meet a pulsed power system's requirements, the BMS performs three functions: charging lithium-ion batteries, storing energy for the pulsed power application in lithium-ion batteries, and discharging the energy in pulses to simulate the requirements of a pulse power system. To perform these three functions the BMS has several elements to include the power source, the charger, the batteries, the FPGA controller, and the discharge mechanism. The design and construction of the BMS and these individual elements will be explored in detail in this thesis.

THIS PAGE INTENTIONALLY LEFT BLANK

TABLE OF CONTENTS

LIST OF FIGURES

THIS PAGE INTENTIONALLY LEFT BLANK

LIST OF TABLES

THIS PAGE INTENTIONALLY LEFT BLANK

LIST OF SYMBOLS, ACRONYMS, AND ABBREVIATIONS

A	Amperes
BMS	Battery Management System
BNC	Bayonet Neill-Concelman
CC	Constant Current
CCCV	Constant Current Constant Voltage
CV	Constant Voltage
D	Duty Cycle
DC	Direct Current
EDLC	Electric Double Layer Capacitors
FPGA	Field Programmable Gate Array
Hr	Hour
J	Joules
Li-ion	Lithium-Ion
NPS	Naval Postgraduate School
V	Volts
PCB	Printed Circuit Board
PI	Proportional–Integral
PWM	Pulse Width Modulation
MOSFET	Metal Oxide Semiconductor Field Effect Transistor
OPAMP	Operational Amplifiers
RMS	Root, Mean, Square
SMES	Superconducting Magnetic Energy Storage
TC	Trickle Charging
W	Watts

THIS PAGE INTENTIONALLY LEFT BLANK

EXECUTIVE SUMMARY

The work documented in this thesis realizes a small-scale implementation of a Battery Management System (BMS) that has the charging, storage, and discharge capabilities to meet scaled down requirements of a pulsed power system. Further, this work establishes a flexible battery research and testing capability resident at the Naval Postgraduate School (NPS). The designed architecture will provide this flexibility by providing the capability to change charging methodologies and types of batteries with only a change of the FPGA software.

Several specifications about pulsed power systems must be known in order to fully define the system. The first specification would be the level of power required during each of the pulses. Another specification necessary to define the system is the number of times this pulse is required to be repeated. Also required is the period of these pulses. The number of repeated pulses, the power level of these pulses, and the period of these pulses will then determine the system's energy storage requirements. Additionally, the space that the energy storage medium can occupy must be known. This last specification will be called the energy density for this system. Once these five specifications are known, possible solutions to these requirements can be developed.

The following table summarizes the required specifications to completely develop a solution to pulsed power applications. These requirements could also include the total weight of the pulsed power system; however, due to the capabilities of U.S. Navy ships, weight can be disregarded as it is the least limiting factor for system solutions.

System Requirement	Description
Power Rating	The rate of electrical energy delivered during the pulse.
Pulse Repetitions	The number of pulses required.
Pulse Period	Length of the pulse duration.
Energy Storage Required	The total amount of stored energy to meet the power and pulse requirements.
Energy Density Requirement	The amount of energy in a certain volume.

Pulsed Power System Requirements

This thesis demonstrates a scaled pulse power system using lithium-ion batteries as the energy storage medium and uses one charger per battery for maximum charging flexibility. A basic functional diagram of the BMS is shown in the following figure.
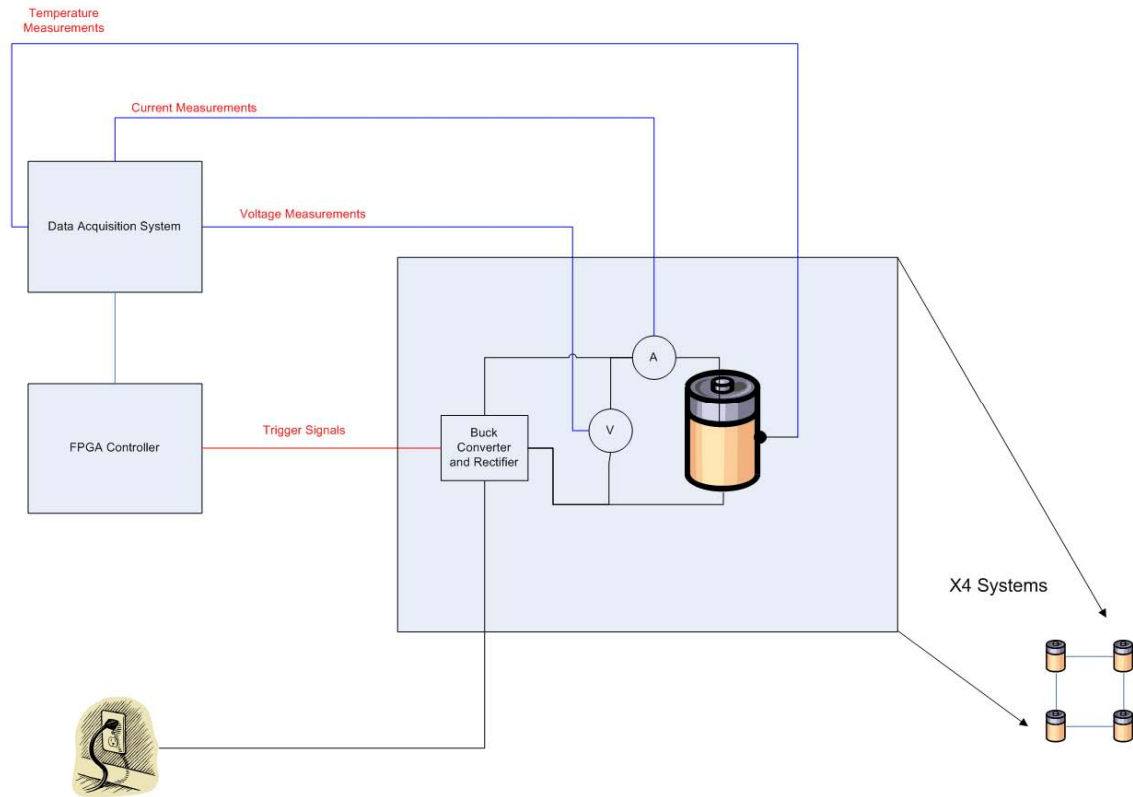
Functional Diagram of the BMS.

In order to meet a pulsed power system's requirements, the BMS performs three functions: charging lithium-ion batteries, storing energy for the pulsed power application in lithium-ion batteries, and discharging the energy in pulses to simulate the requirements of a pulse power system. To perform these three functions, the BMS has several elements to include the power source, the charger, the batteries, the FPGA controller, and the discharge mechanism. These elements have been collected into three components for the purpose of this design. These components, as shown in the next figure, are the power source and discharge component, the charger, and the FPGA controller. The design and construction of the BMS and these individual components will be explored in detail in this thesis.
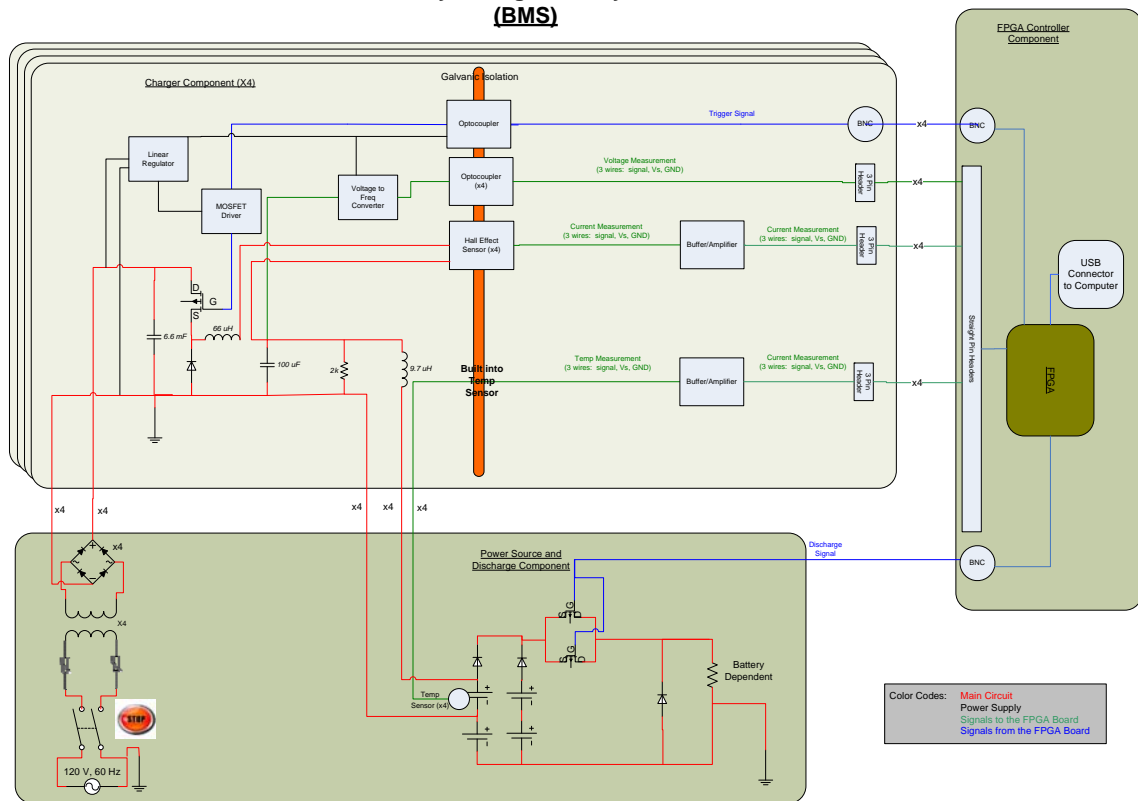
Battery Management System Components.

I.   INTRODUCTION

A.   PULSED POWER

The United States Navy uses many electrical systems that require or produce pulsed power. For the purposes of this thesis, pulsed power will be defined as high power levels delivered over short periods or pulses. To fully define a pulsed power system, several specifications about the system must be known. The first specification would be the level of power required during each of the pulses. Another specification necessary to define the system is the number of times this pulse is required to be repeated. Also required is the period of these pulses. The number of repeated pulses, the power level of these pulses, and the period of these pulses will then determine the system's energy storage requirements. Additionally, the space that the energy storage medium can occupy must be known. This allowable space and the energy that the storage medium can accommodate in this space will be used to determine the energy density for this system. Once these five specifications are known, possible solutions to these requirements can be developed.

Table 1 summarizes the required specifications to develop a solution to pulsed power applications. These requirements could also include the total weight of the pulsed power system; however, do to the capabilities of U. S. Navy ships, weight can be disregarded as it is the least limiting factor for system solutions.

| System Parameter	Description
Power Rating	The rate of electrical energy delivered during the pulse.
Pulse Repetitions	The number of pulses required.
Pulse Period	Length of the pulse duration.
Energy Storage Required	The total amount of stored energy to meet the power and pulse requirements.
Energy Density Requirement	The amount of energy in a certain volume.

Table 1.   Pulsed Power System Requirements.

Pulsed power requirements for an example Navy system are listed in Table 2. The specification for the energy density requirement is left generic since this requirement is difficult to quantify. Instead, the highest energy density will be considered for the system that meets the specifications for the other requirements. With these pulse power requirements, a solution can be developed.

System Parameter	Requirement
Power Rating	2 MW
Pulse Repetitions	Ten repetitions of 8-second pulses. One pulse will be required every 10 seconds.
Energy Storage Required	16 MJ (4.4 kWh)
Energy Density Requirement	High energy density.

Table 2.   Pulsed Power System Specifications.

B. ENERGY STORAGE MEDIUM

The first step in developing a solution to this pulsed power system is to determine the energy storage medium. Once the medium that will store and provide the energy is determined, other aspects of this pulsed power system can be developed.

First, the power rating specification for this pulsed power system will be considered. Figure 1 shows the power rating versus discharge time for recently installed energy storage systems. The red box on Figure 1 indicates the approximate desired specifications of the desired pulsed power system. As can be seen in this figure, several solutions are possible that provide the necessary power levels such as using a flywheel or various types of batteries including lead-acid, nickel-cadmium, lithium-ion (Li-ion), and nickel-metal hydride.
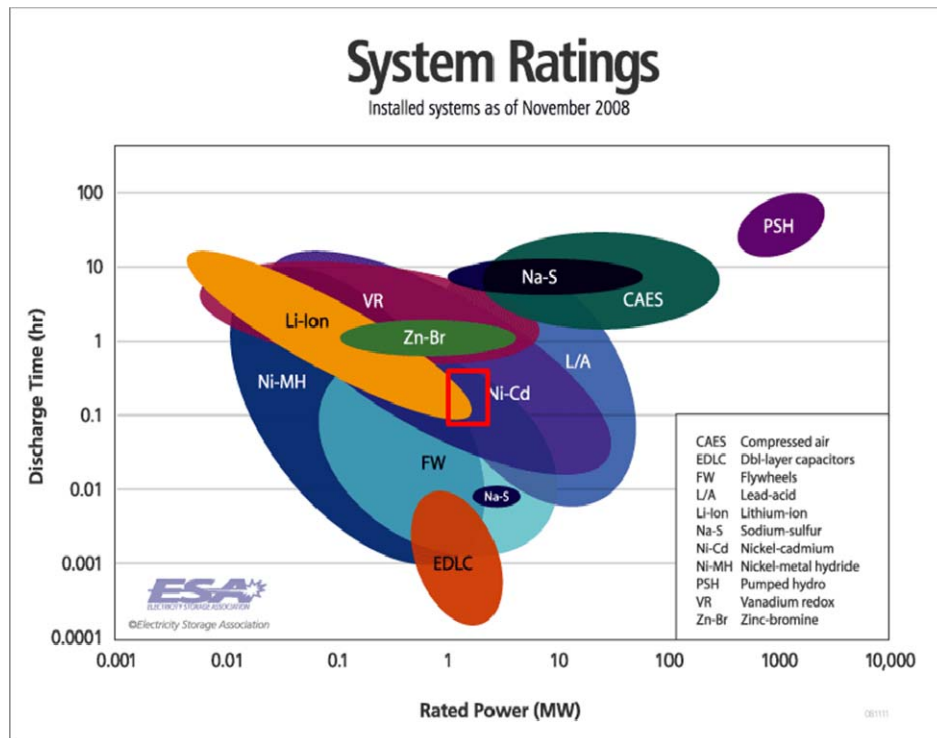
Figure 1.   Power Ratings of Recently Installed Energy
Storage Systems. From [1].

Secondly, the energy storage specifications for this pulsed power system will be considered. Figure 2 shows the energy storage ratings versus power for recently installed energy storage systems. The red box on Figure 2 indicates the desired energy storage specifications for the pulsed power system. The following list explains the terminology used in this figure.

- Conventional: lead-acid, nickel-cadmium, and nickel-metal hydride batteries.
- Lithium: lithium ion batteries.
- Flow: zinc-bromine and vanadium redox batteries
- NAS: high-temperature sodium batteries
- EDLC: Electric Double-Layer Capacitors
- SMES: Superconducting Magnetic Energy Storage

As can be seen from Figure 2, several solutions are possible to meet the energy storage requirements of this pulsed power system including EDLCs, flywheels, and Li-ion batteries.
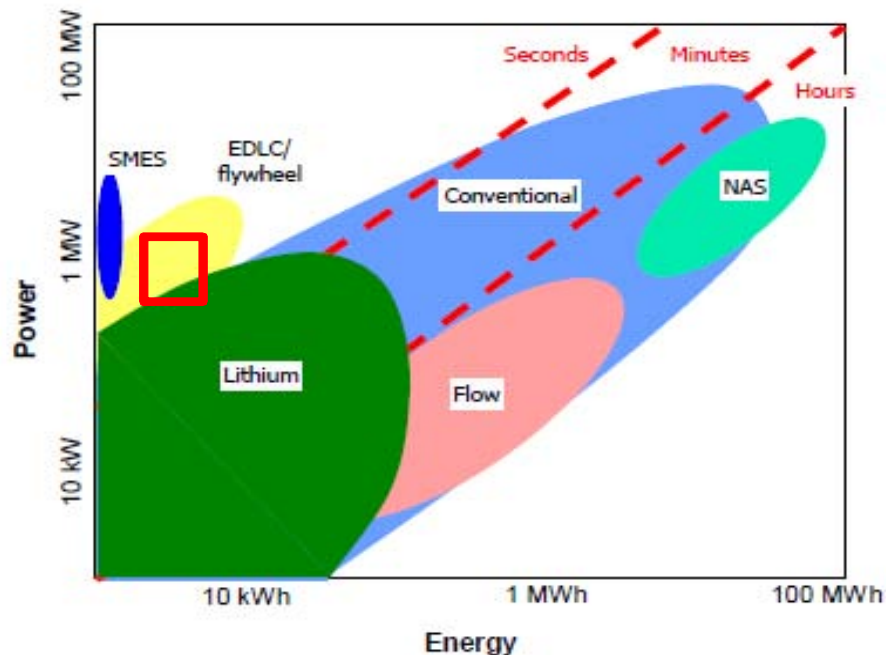
Figure 2. Energy Ratings of Recently Installed Energy Storage Systems. From [2].

4

Since the pulse repetition requirement and the pulse period were used to determine the total energy storage requirement, these can be added to the requirements already analyzed for this pulsed power system. After this analysis of four of the five pulse power system requirements, the number of possible solutions has been limited to only a few. Only flywheels and Li-ion batteries meet the first three system requirements. To determine which one of these solutions best meets this system's requirements, the last requirement, energy density, will be analyzed.

Figure 3 shows the volume energy density and weight energy density of current energy storage technologies. As previously discussed, only the volume energy density is of interest in determining suitability for this pulse power system. If the two candidate energy storage mediums are compared using Figure 3, Li-ion batteries become the preferred solution for this pulsed power system. Li-ion batteries provide a much higher energy density and therefore would occupy significantly less space than an equivalently sized flywheel storage medium.
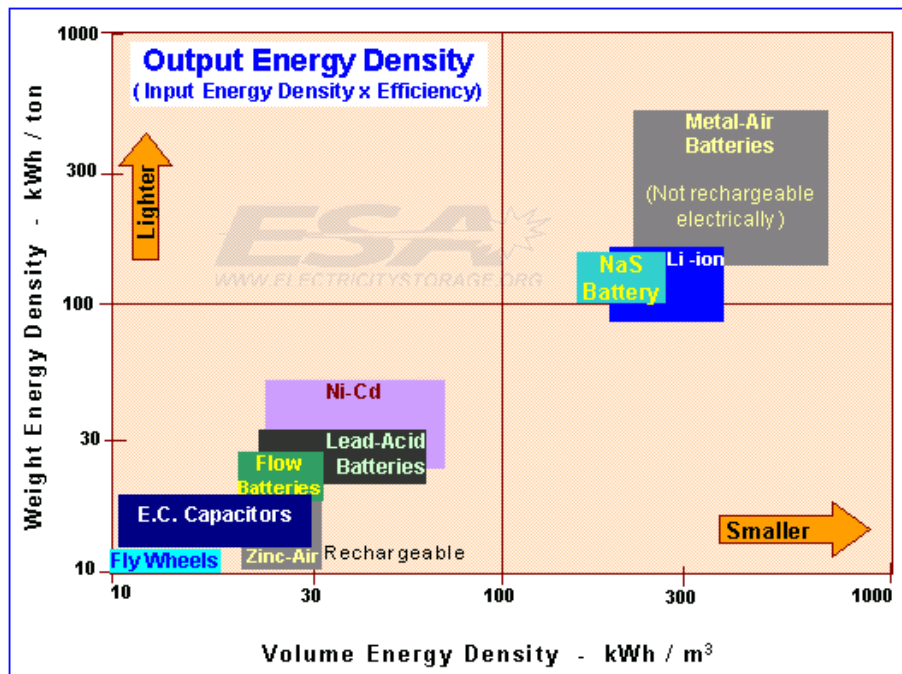
Figure 3.   Output Energy Density of Current Energy Storage Technologies. From [3].

5

With the energy storage medium chosen the next step in developing a solution to this pulse power system is to determine the method of charging the Li-ion batteries.

C. CHARGING METHODOLOGY

1. Charging Limitations

While Li-ion batteries provide a high energy density and power rating compared to other storage mediums, they do have limitations. In particular, here are the issues:

- The voltage in a Li-ion battery cell is usually low. Voltage ratings at full capacity for modern high-power Li-ion batteries are in the range of 3.3 V to 4.2 V. Typically, pulse power applications require much higher voltages which means stringing multiple Li-ion cells in series. The strings of cells complicate the overall system architecture and complicate the charging of Li-ion batteries [4].

- Li-ion batteries are very sensitive to overcharging and overdischarging. Specifically, overcharging with either too high a voltage or too high a current could either ignite the overcharged battery cell or even cause an explosion. Overdischarging a Li-ion cell through too much current can again cause a fire or explosion while overdischarging a cell below the manufacturers minimum discharge voltage can permanently damage the cells internal chemistry. This damage will reduce the capacity and lifetime of the affected cell [4], [5], [6].

- Probably the most important limitation of Li-ion batteries is the strict requirement of managing charge equalization in battery strings. Partially resulting from the above listed Li-ion battery sensitivities and partially due to varying levels of increasing internal resistance in cells developed during repeated discharge and charge cycles, the voltage of individual Li-ion batteries in strings must be independently monitored.

6

For Li-ion batteries, it is not sufficient to monitor only the battery pack or string voltages [4], [5].

2. Charging Methods and Architectures

Various methods exist to charge Li-ion batteries. All the methods must take into account the sensitivities of these cells. Different methods include multi-stage constant current charging, pulse charging, and constant current, constant voltage (CCCV) charging. The first two listed methods reduce charging times for Li-ion batteries but are typically complex strategies to implement. The last charging method, CCCV, while taking longer to fully charge the battery, is simpler to implement and more readily stays within manufacturer's current and voltage charging limitations [5], [6], [7], [8], [9]. Because of this method's simplicity and safety, it will be used as the charging algorithm for the proposed pulse power system.

Before the CCCV charging technique can be discussed, important manufacturer-provided characteristics of lithium-ion batteries must be introduced. Each of these characteristics must be known to safely charge and discharge any lithium-ion battery.

One important battery characteristic is capacity. This value is usually given in A-hrs and is a rough energy-like measurement of the total energy capacity of the battery. The true energy capacity for the battery is determined by multiplying the capacity value by the non-linear discharge voltage that depends upon the discharge current. The next battery characteristic is the maximum continuous discharge current. As the name indicates, this value should not be exceeded for continuous discharge of the battery. Damage could result if this value is exceeded. Another characteristic of lithium-ion batteries is the current rating during the constant current (CC) stage of the charge cycle. This value is the maximum intended current level during continuous charging of the battery. The next characteristic is voltage rating during the constant voltage (CV) stage of the charge cycle. This value is the maximum continuous voltage level to

7

maintain during the charging of the battery. Another characteristic is the cutoff charge current. This is the lowest level that the charge current should be allowed to fall to during the constant voltage stage of charging. This is the traditional indicator that the CCCV charging process is complete. A final lithium-ion characteristic is the discharge cutoff voltage. This is the lowest level that the battery voltage should be allowed to drop to during discharge. This voltage level indicates that the entire capacity has been discharged and any further discharge could permanently harm the internal chemistry of the battery. Table 3 summarizes these common lithium-ion battery characteristics [5], [7], [9].

Battery Characteristic (Units)	Purpose
Capacity (A-hr)	General energy-like measurement for the energy stored in a battery.
Maximum Continuous Discharge Current (A)	This is the maximum continuous current that should be allowed during the discharge of the battery.
CC Current Rating (A)	Maximum continuous current during the CC stage of charging.
CV Voltage Rating (V)	Maximum constant voltage during the CV stage of charging.
Charge Cutoff Current (A)	Lowest current that the battery should be allowed to reach during the CV stage of charging. This characteristic indicates the end of the CCCV charging process.
Discharge Cutoff Voltage (V)	Lowest voltage that the battery should be allowed to reach during the discharge of the battery. This characteristic indicates that the entire capacity of the battery has been expended and further discharge could permanently damage the battery.

Table 3.   General Lithium-Ion Battery Characteristics.

The CCCV charging method involves three different stages of battery charging. The first stage, trickle charging (TC), uses a current of 10% of the manufacturer's normal charging current to bring the cell up to the discharge cutoff voltage. Reasons for the battery to be below this value are excessive discharging of the battery or when first charging a new battery. The next stage of CCCV charging is the constant current stage. During this stage, the battery is charged at a constant current level until the battery reaches the CV voltage rating. During this second stage, the battery typically attains around 70% of the total capacity of the battery. The final stage of CCCV charging is the constant voltage stage. During this stage, a constant voltage is applied until the charging current falls to the charge cutoff current level. Even though less of the capacity of the battery is attained during this last stage, this stage typically takes much longer than the second stage due to less current flowing to the battery [5], [7], [8], [9].

Figure 4 shows typical current, voltage, and capacity curves for a lithium-ion battery during the CCCV charging process. For this figure, the charge voltage for the CV stage is 4.2 V, the charge current for the CC stage is 1.3 A, and the charge cutoff current is 0.10 A. Per the previous discussion, Figure 4 shows the majority of the capacity of the battery is gained during the CC stage of charging.
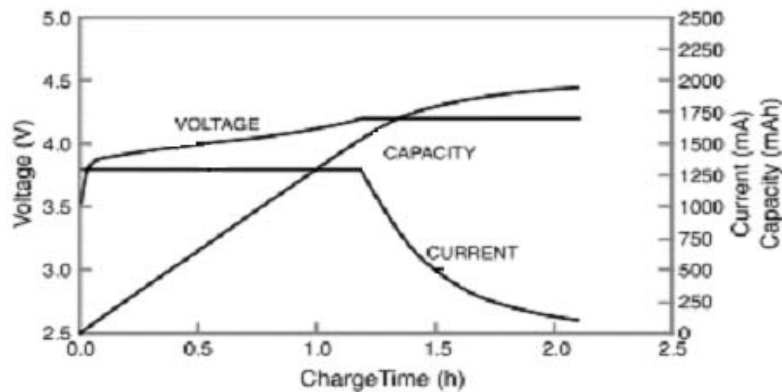
Figure 4.   CCCV Charging Process. From [10].

9

Numerous different architectures are possible when charging lithium-ion batteries. The primary requirement for and limitation on these architectures is the requirement to equalize charge among battery cells in series strings. These various architectures generally can be collected into four groups: parallel/taper charging, series charging/cell shunting, resistive equalization, and transformer equalization. All of these methods rely on using either resistive means to dissipate energy from the highest charged batteries to equalize them with lower charged batteries or using complex converters, switches, or transformer/capacitive circuits to recycle the energy from the highest charged battery to the lowest charged battery [5], [6], [11], [12].

To alleviate the complexities and/or the resistive losses of charge equalization, a non-traditional architecture will be used in this proposed pulsed power system design. This solution will use a transformer, rectifier, and a buck converter as a charger for each battery. Charge equalization will be inherent in this system as each individual charger will control the CCCV process for its battery. The drawbacks of this system are the expense of having one charger per battery and the space requirement to have one charger per battery. Both drawbacks can be lessened with increasing the energy storage and power ratings of the charged batteries. The drawbacks of this architecture lessen with an increase in the battery's capabilities.

Figure 5 shows a simple functional diagram of the charging portion of the proposed pulsed power system design. As discussed, each battery will have an individual charger. The proposed system will charge two parallel strings of two batteries in series. This battery arrangement ensures that the complexities of charging strings and then strings in parallel of lithium-ion batteries are encountered and overcome in the design. A Field Programmable Gate Array (FPGA) will use signals from each battery and charger to control the CCCV charging process. This system will be discussed in significantly more detail in the following chapter.
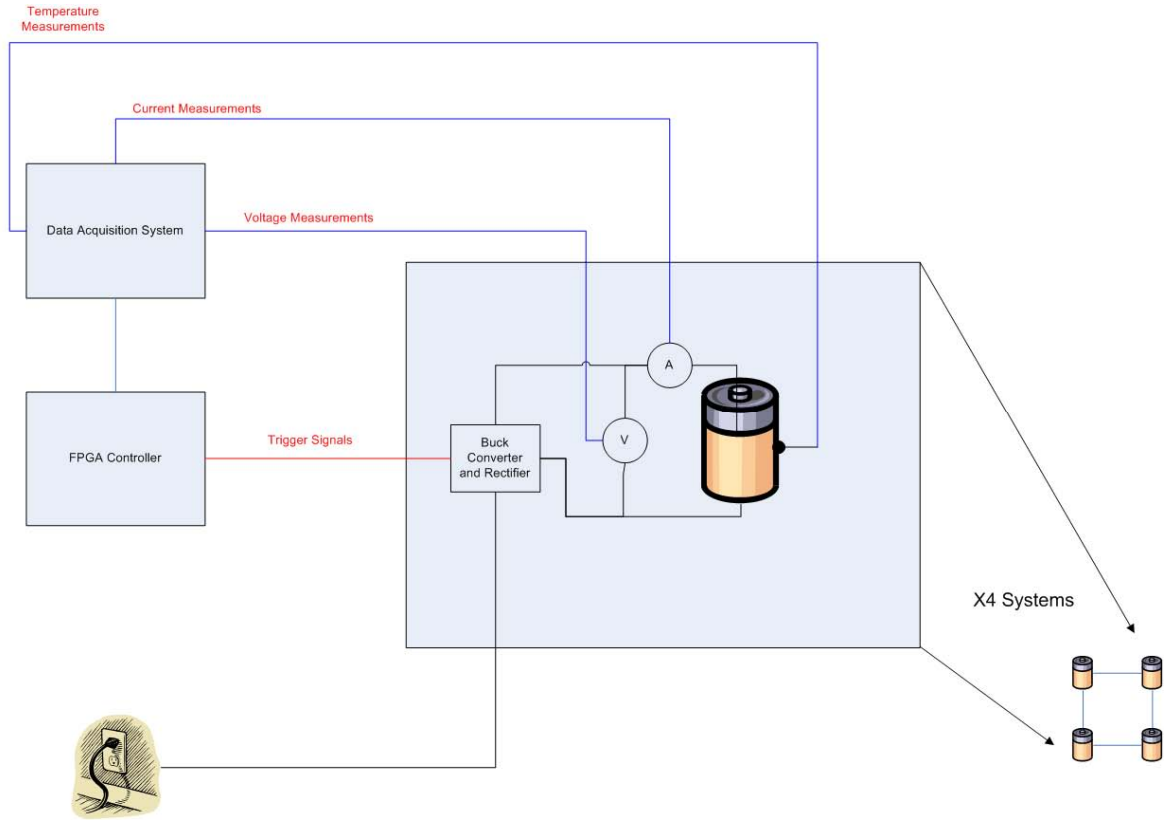
Figure 5.   Functional Diagram of the Battery Management System.

D.   THESIS GOALS

The first research goal was to survey the literature to determine which currently available energy storage technologies were capable of meeting system requirements. The second goal was to select one energy storage technology for further development. The third goal was to design, build, and test a system for charging, storing, and discharging energy, using the selected energy storage technology.

E.   THESIS STRUCTURE

- Chapter I introduces the pulsed power problem and proposes a possible design to meet the identified requirements.

- Chapter II discusses the theory of operation of the BMS and reviews the Simulink® model developed for this system.

11

- Chapter III explores the construction, assembly, and testing of the BMS.

- Chapter IV addresses the results and conclusions of the BMS operation and recommends future research efforts related to the BMS.

- Appendix A contains the operational safety procedures developed to operate the BMS.

- Appendix B contains the Simulink® model and its associated MATLAB® code.

F.   CHAPTER SUMMARY

Many different requirements can be used to determine the appropriate energy storage medium and charging methods for pulse power applications. Five of these possible requirements have been reviewed and used to develop a design for this pulse power application. These requirements directly led to the choice of lithium-ion batteries as the storage medium while simplicity and controllability led to the choice of the one-charger-per-battery solution for the charging architecture and the use of the CCCV charging process. The next chapter will review the theory of operation for this BMS and will discuss its associated Simulink® model.

II.   THEORY OF OPERATION AND MODEL

A.   INTRODUCTION

This chapter will discuss the theory of operation of the BMS and will review the model developed for the charging function of the BMS. The theory of operation discussion will detail the operation of the individual components of the BMS, their interaction with other components, and the signals used for controlling the charging and discharging processes in the BMS. The discussion of the model will focus on the model developed for the controller, buck converter, and the battery.

B.   THEORY OF OPERATION

1.   Overview

The BMS is intended as a small-scale solution to the requirements identified in Chapter I. In order to fulfill these requirements, the BMS performs three functions: charging lithium-ion batteries, storing energy for the pulsed power application in lithium-ion batteries, and discharging the energy in pulses to simulate the requirements of a pulse power system. To perform these three functions the BMS has several elements to include the power source, the charger, the batteries, and FPGA controller, and the discharge mechanism. These elements have been collected into three components for the purpose of this design. These components, as shown in Figure 6, are the power source and discharge component, the charger, and the FPGA controller. These individual components will be discussed in the following paragraphs.

Battery Management System (BMS)

Figure 6.   Battery Management System Components.
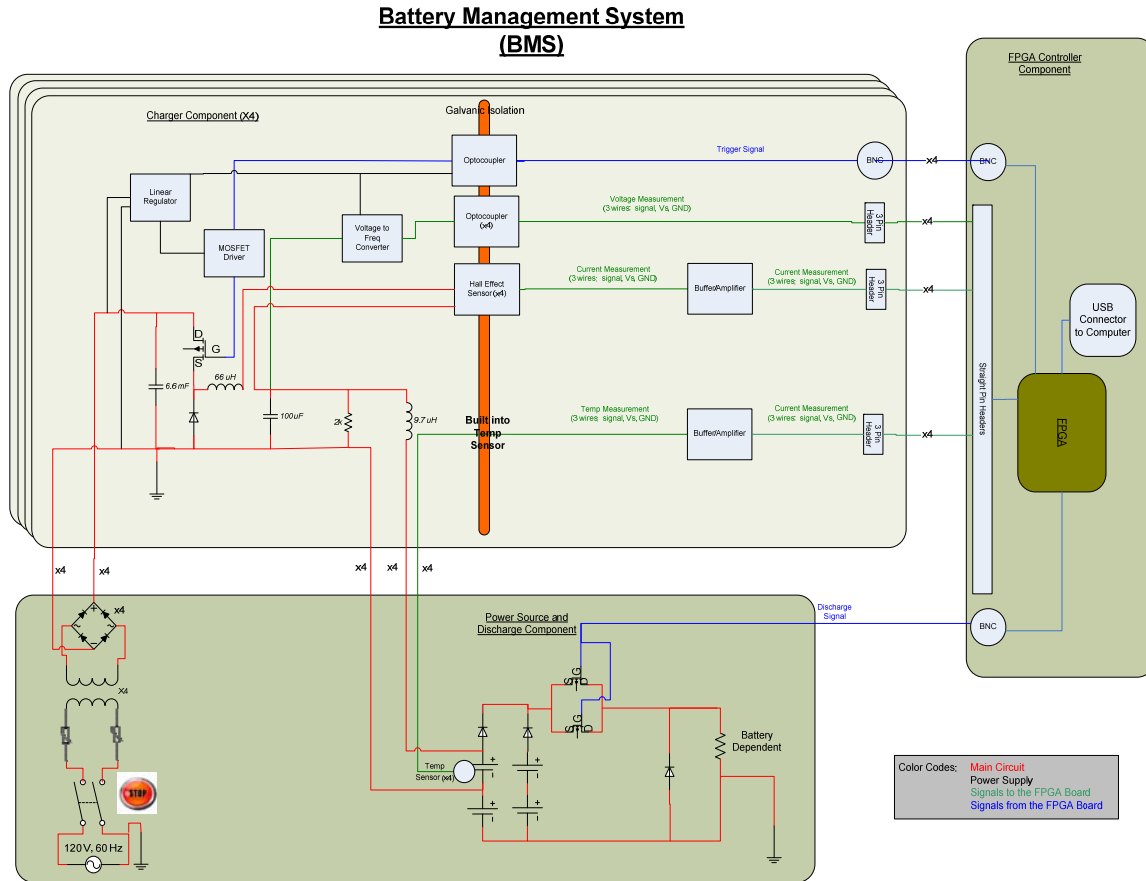
2.   BMS Components

a.   *Charger Component*

The charger component's primary function, as the name implies, is to charge the lithium-ion batteries. To accomplish this goal, the charger contains several pieces to include the smoothing capacitor, the buck converter, the on-board power supply, and the pieces necessary to route the signals from the buck converter to the FPGA. Together, these parts provide the BMS with the charging capabilities as listed in Table 4. These pieces will be discussed in detail in the following paragraphs.

Maximum Charging Voltage	Maximum Charging Current
4.5 V	10 A

Table 4.   BMS Charging Capabilities.

Buck Converter. This converter topology was chosen due to its relative simplicity of design, broad range of voltage and current capabilities, and its exceptional efficiency. The drawbacks to a buck converter include its larger size and higher noise production than other types of converters [13], [14], [15].

The buck converter, as shown in Figure 7, includes a power MOSFET switch, a free-wheeling diode, an LC filter made up of the 66 uH inductor and the 100 uH capacitor, and a $2\,k\Omega$ resistor. This converter is a type of switch-mode DC power supply that converts unregulated DC input into a controlled DC output at a desired voltage level [16]. The buck converter's design is such that it produces lower voltage output to the load that it receives as an input to the switch. It steps-down or bucks the input voltage. This reduction of the average voltage level is accomplished by turning the power MOSFET on and off at a frequency and duty cycle to produce the desired, regulated output.
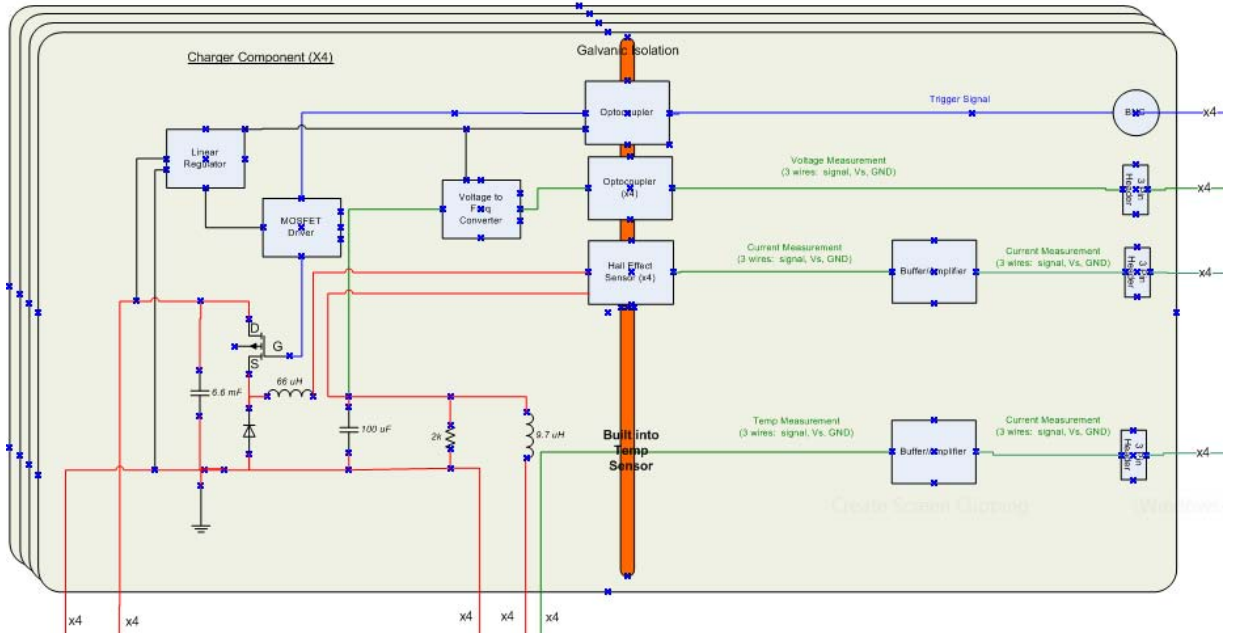
Figure 7.   Charger Component of the BMS.

Although varying both the frequency and duty cycle can be used to produce regulated voltage or current levels, the buck converter for this pulsed power system solution will switch at a constant frequency of 30 kHz. Since the switching frequency will be constant, the duty cycle, as defined by equation (2.1), will be used to produce the desired output levels. In equation (2.1), t_{on} is the time that the switch remains on and *T* is the switching period. This method of varying the regulated voltage or current levels was chosen for the simplicity of control and for the ease of determining appropriate inductor and capacitor values for the converter LC filter [13], [16]. The actual control methodology for this buck converter will be discussed in the model portion of this chapter.

$$Duty\ Cycle\ (D) = \frac{t_{on}}{T} \tag{2.1}$$

Buck converters can operate in both continuous and discontinuous conduction modes depending upon the consistency of the flow of current through the converter inductor. A constant flow of current is continuous conduction while

16

any regular stoppage in current flow during the switching periods is considered discontinuous conduction [13], [16]. In order to apply the CCCV charging process, both continuous and discontinuous conduction modes will be used in this converter. At higher duty cycle values the converter will operate in continuous conduction mode while the converter will enter discontinuous conduction when at lower duty cycle operation.

In order to provide general equations for the operation of this buck converter, several assumptions must be made. First, the switch will be considered ideal when in the "on" position. No power will be dissipated by this device. Second, the diode will be considered ideal when it is forward biased. No voltage drop will be considered for this device. Finally, the load for the converter will be represented with a 9.7 uH inductor and a voltage source representing the battery. The reason for the inclusion of the 9.7 uH inductor as part of the converter load will be discussed in the next chapter. While these assumptions mean that the following equations will not perfectly describe the designed system, they are necessary to produce generalized equations for this converter. With these assumptions, the converter circuit can be represented by a simplified circuit as seen in Figure 8.
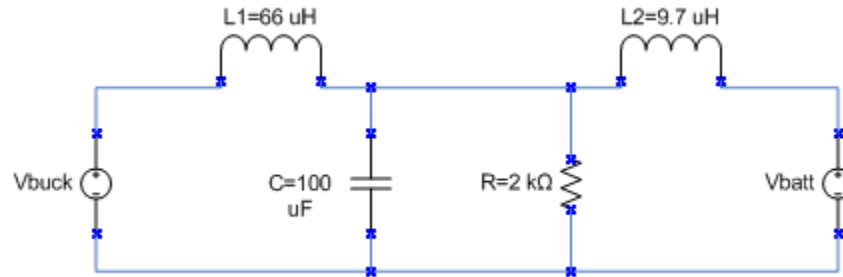
Figure 8.   Simplified Converter Circuit.

The first general equation for this simplified buck converter circuit is equation (2.2). In equation (2.2) V_c is the voltage provided to the converter load and V_{in} is the voltage provided to the converter switch. This equation shows a

17

simple, linear relationship between the average input voltage and the average output voltage. To control the level of the output, only the duty cycle (D) needs be varied. This simple, linear relationship exists because the inductors have no average voltage loss during steady state operation [16], [17], [18].

$$V_C = DV_{in} \qquad (2.2)$$

The next general equations for the buck converter are listed as equations (2.3), (2.4), (2.6), and (2.7). These equations are the transfer functions and associated state space representations for both of the voltage sources, V_{buck} and V_{batt}, to the output of the converter, V_C. Since these two voltage sources are linearly independent, the total output of the converter would be found by combining the results of the two voltage sources. Since the simplified circuit of the converter contains three energy storage elements, the transfer function is third order or similarly the state space representation has three state variables as listed in equation (2.5).

$$\frac{V_C}{V_{buck}} = \frac{sRL_2}{s^3 RL_1 L_2 C + s^2 L_1 L_2 + s(RL_2 + RL_1)} \qquad (2.3)$$

$$\frac{V_C}{V_{batt}} = \frac{sRL_1}{s^3 RL_1 L_2 C + s^2 L_1 L_2 + s(RL_1 + RL_2)} \qquad (2.4)$$

$$\dot{\vec{x}} = \begin{bmatrix} I_{L1} \\ I_{L2} \\ V_C \end{bmatrix} \qquad (2.5)$$

18

$$\dot{\vec{x}} = \begin{bmatrix} 0 & 0 & -\dfrac{1}{L_1} \\[2mm] 0 & 0 & \dfrac{1}{L_2} \\[2mm] \dfrac{1}{C} & -\dfrac{1}{C} & -\dfrac{1}{RC} \end{bmatrix} \vec{x} + \begin{bmatrix} \dfrac{1}{L_1} \\[2mm] 0 \\[2mm] 0 \end{bmatrix} V_{buck} \qquad (2.6)$$

$$\dot{\vec{x}} = \begin{bmatrix} 0 & 0 & \dfrac{1}{L_1} \\[2mm] 0 & 0 & -\dfrac{1}{L_2} \\[2mm] -\dfrac{1}{C} & \dfrac{1}{C} & -\dfrac{1}{RC} \end{bmatrix} \vec{x} + \begin{bmatrix} 0 \\[2mm] \dfrac{1}{L_2} \\[2mm] 0 \end{bmatrix} V_{batt} \qquad (2.7)$$

In order to filter the 30 kHz switching frequency from the output of the converter and thereby provide less ripple in the converter output, the converter contains an LC filter. The corner frequency of this filter was chosen to be at least one order of magnitude less than the switching frequency. This corner frequency, as calculated with equation (2.8), was 1.96 kHz [16], [19]. This method of calculating the corner frequency provides another general equation to describe this buck converter.

$$f_c = \frac{1}{2\pi\sqrt{LC}} \qquad (2.8)$$

The final general equations used to describe the functioning of the converter are approximations for the current and voltage ripple of the converter output. Equations (2.9) and (2.10) were produced through a geometric argument using the current waveform through inductor and the output voltage waveform as detailed in [16]. The two requirements to use these approximations are a constant average voltage being applied to the output and for the converter to be in continuous conduction mode. These requirements therefore cause equations

19

(2.9) and (2.10) to apply to this converter during only part of its operations. Using an average output voltage of 3.5 V, a duty cycle of 35%, and a switching frequency of 30 kHz produced expected peak-to-peak voltage and current ripples of 47.9 mV and 1.15 A. When charging at 3.5 V, this ripple is approximately 1.4% of this voltage. If charging at the maximum charge current of 10 A, this ripple would be approximately 12% of this current.

$$\Delta V_o = \frac{1}{C}\frac{1}{2}\frac{\Delta I_{L1}}{2}\frac{T_s}{2} \tag{2.9}$$

$$\Delta I_{L1} = \frac{V_o}{L_1}(1-D)T_s \tag{2.10}$$

Besides the power MOSFET and the LC filter, as discussed in the above general converter equations, the converter also contains other components. These include the freewheeling diode and the bleed resistor. The freewheeling diode provides a current path for the converter inductor, L1, as seen in Figure 9, when the switch opens. Without this current path, the voltage would quickly build up on the inductor with the rapid fall of the current [14], [18]. This large reverse voltage would likely damage the power MOSFET switch. The bleed resistor is meant to help dissipate any residual energy stored in the circuit upon completion of operation of the converter. The high value of resistance and low charging voltages ensures that little current is lost from the converter to the battery during charging operations.

Smoothing Capacitor. The smoothing capacitor, shown on the left side of Figure 9 as the 6.6 mF capacitor, smoothes the unregulated power provided by the power source and discharge component to the converter. This large capacitor ensures that very low ripple DC power is provided to the converter [13], [16], [17].

On-board Power Supply. Three devices in the charger component require a power from the converter in order to perform their function. These devices are the driver for the MOSFET switch, the voltage to frequency converter in the voltage measurement signal, and the trigger or switching signal optocoupler. These devices are all powered by the linear regulator seen in Figure 9. This linear regulator provides a stable 5 V to the charger devices while drawing its own power directly from the output of the transformer on the power source and discharge component. The 2 kΩ resistor in the linear regulator circuit ensures that the linear regulator always has a load and associated minimum current draw that is required for its proper operation [20].

5 V Linear Regulator

+10 Volts DC from Transformer

Linear Regulator

1 uF

2k   1 uF

+5 Volts to MOSFET driver
+5 Volts to Voltage to Frequency Converter
+5 Volts to the Trigger Signal Optocoupler
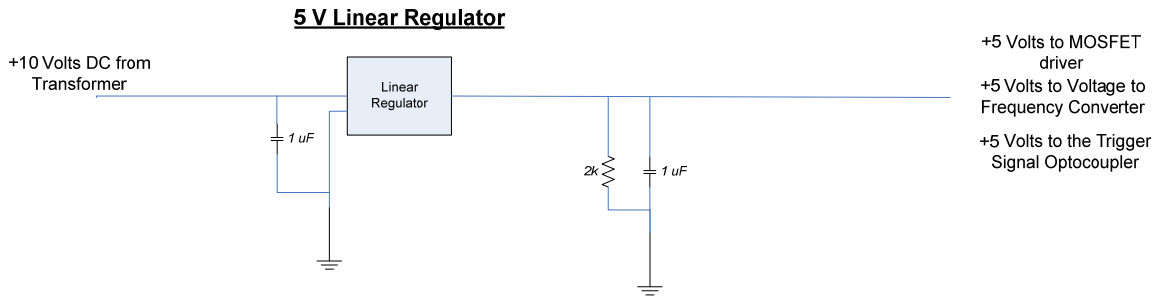
Figure 9.   Charger Internal Power Source.

Trigger or Switching Signal. The trigger signal is brought to the charger via a BNC connector. This signal, as seen in Figure 10, first is galvanically isolated with an optocoupler and then routed to the MOSFET driver. This driver then closes the MOSFET switch as indicated by the trigger signal. This signal provides the control mechanism to change the duty cycle of the converter thereby changing the level of voltage or current produced by the converter.
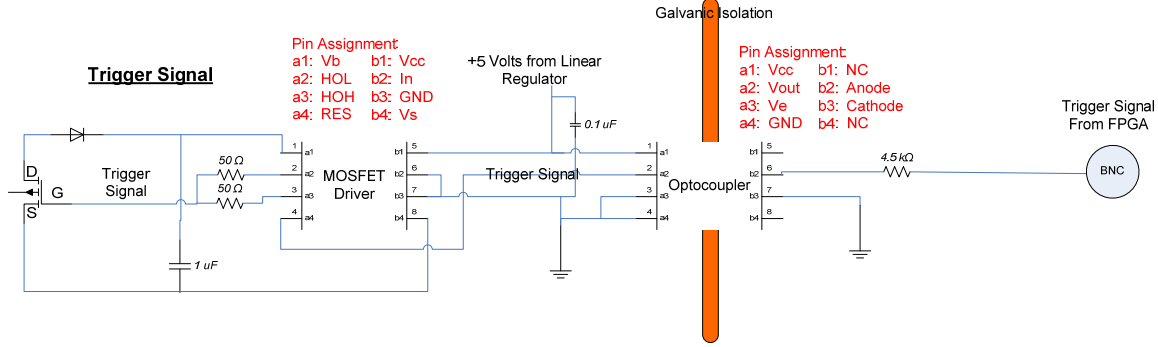
Figure 10.   Trigger Signal.

Voltage Measurement. The voltage measurement for each charger is taken across the 100 uF capacitor that is part of the filter of the converter. This voltage measurement, as seen in Figure 11, is first converted to a frequency value per equation (2.11) by a voltage to frequency converter and then sent to an optocoupler [21]. This measurement leaves the voltage to frequency converter as a square wave. As in the trigger signal, the optocoupler provides this signal with galvanic isolation. The signal then leaves the charger via a 3 pin header connector.
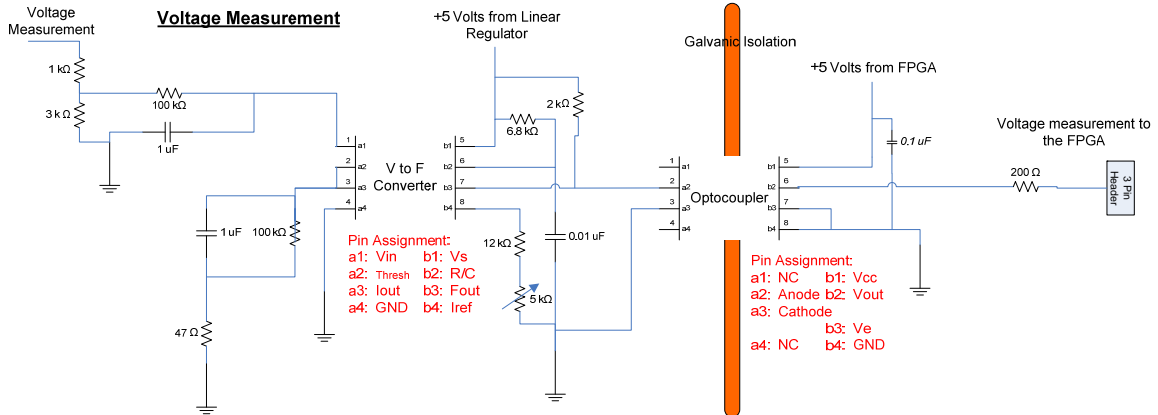
Figure 11.   Voltage Measurement Signal.

$$f_{out} = \frac{V_{in}}{2.09\,V}\frac{R_s}{R_L}\frac{1}{R_t C_t}$$ (2.11)

The values of the variables in equation (2.11), as taken from Figure 11, are seen in the following list.

- V_{in} is the measurement voltage into the voltage to frequency converter.
- R_s is the combination of the 12 kΩ resistor and the 5 kΩ potentiometer. The value for this device as set on charger #1 is 770 Ω.
- R_L is the 100 kΩ resistor that is in parallel with the 1 uF capacitor.
- R_t is the 6.8 kΩ resistor.
- C_t is the 0.01 uF capacitor.

Current Measurement. The current measurement is the current value through the inductor of the converter. This measurement is taken using a Hall Effect sensor that also provides inherent galvanic isolation for this signal. Due to the low voltage returned by the Hall Effect sensor at the expected range of charge currents as determined by equation (2.12) [22], the signal is then buffered and amplified with a non-inverting OPAMP. This OPAMP circuit has a gain of 1.7, which is the maximum value that could be used to not exceed the input saturation voltage of this circuit. The current measurement signal is shown in Figure 12.
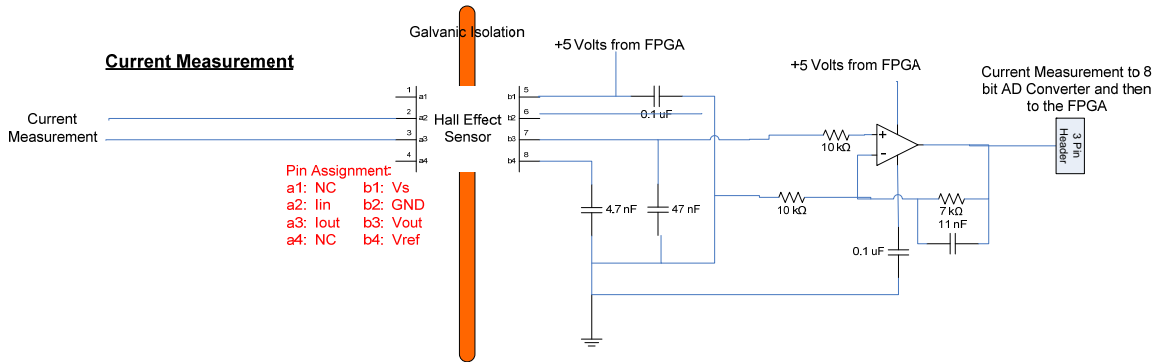
Figure 12.   Current Measurement Signal.

$$V_{out} = 2.5 + 0.626 \frac{I_{meas}}{20} \tag{2.12}$$

Beyond just amplifying and buffering the current measurement, the capacitor used in the feedback path of the OPAMP circuit also serves to filter this signal. The value of the capacitor, 11 nF, was chosen by using equations (2.13) and (2.14) in order to create a corner frequency of 2 kHz [23]. This filter removes most of the switching frequency ripple at 30 kHz and other high frequency noise from this current measurement.

$$H(s) = 1 + \frac{R_f \parallel \frac{1}{sC}}{R_i} = 1 + \frac{R_f R_i}{sCR_2 + 1} \tag{2.13}$$

$$f_c = \frac{1}{2\pi CR_2} \tag{2.14}$$

Galvanic Isolation. Each of the signals to and from the charger has been shown to have galvanic isolation built into the signal circuit. Galvanic isolation in the BMS prevents current from flowing to different components or from and to different chargers that have different ground voltage levels [24]. This isolation is particularly important due to the different ground voltage levels across the chargers of the batteries in series and between the grounds of the other components of the system and the four chargers in the system.

Charger Component Summary. All the parts of the charger component to include the smoothing capacitor, converter, bleed resistor, internal power source, trigger signal, voltage measurement, and the current measurement have been discussed above. It is important to remember that each of these parts is repeated for each of the batteries being charged. For the designed system, four charger components are part of the BMS because four batteries are being charged. The next component of the system, the power source and discharge component, will be next discussed.

### b.	*Power Source and Discharge Component*

While the charger's primary function is to charge the batteries, the power source and discharge component provides unregulated power to the

charger component, provides the energy storage medium for the system, and provides a discharge mechanism for the system. The parts of this component include the power source, the energy storage parts, the discharge parts, and the temperature measurement signal. This component of the BMS is shown in Figure 13. These parts are next discussed.
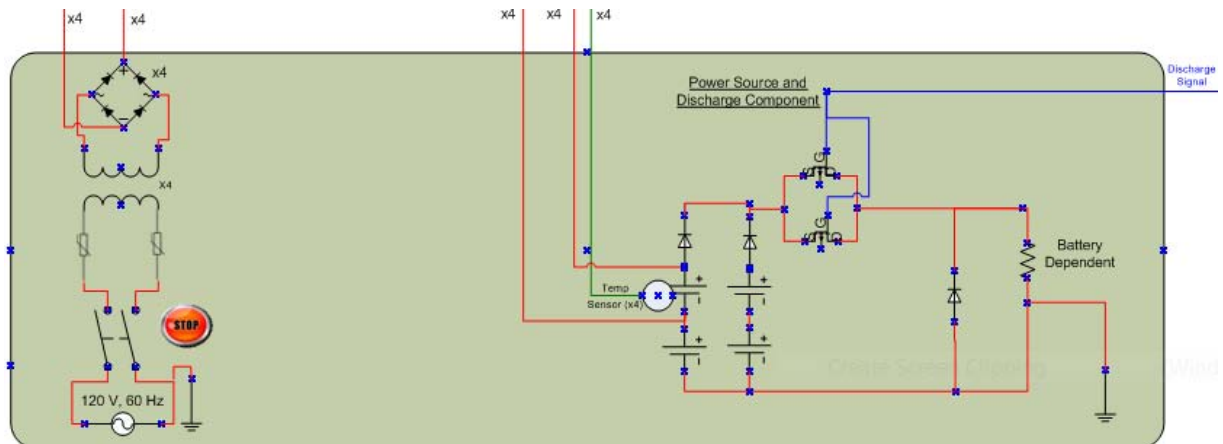
Figure 13.   Power Source and Discharge Component.

Power Source.   The power source for the BMS is provided by a standard wall plug with 120 V, 60 Hz single-phase power. This power is provided directly to a double-throw, normally closed emergency stop switch. If opened, this switch would stop all power from entering the charging system. Two current limiters follow the emergency stop switch. These devices limit the initial surge current when the charger is first energized. As the flowing current causes these devices to warm-up, their resistance drops dramatically thereby limiting their detrimental effect on the power source voltage [25]. From the current limiters, the power flows into the transformers. Each charging component has one transformer on the power source and discharge component. For this design, four transformers take this 120 V AC power and transform it into 10 V AC power at a maximum current of 10 A [26]. This unregulated AC power is then provided to

25

the diode rectifier. These rectifiers, again one per charging component, then provides the unregulated DC power to the smoothing capacitor on the charging component.

Energy Storage. The energy storage mechanism on this component includes the batteries and the diodes on each of the series strings of batteries. The batteries are the storage medium for this pulse power system. The diodes on each of the battery serial strings ensures that an imbalance in voltage across different battery strings does not result in currents flowing from one string into the other.

Energy Discharge. The energy discharge parts of this component include the switches for initiating the discharge, the freewheeling diode, and the load resistors. The switches are high power MOSFET relays, connected in parallel, in order to handle a higher total current than each relay could individual handle. These relays are closed via a signal sent from the FPGA controller component. The freewheeling diode ensures that inductive energy built up in the wires of the discharge wiring can be safely expended in the load resistors while minimizing the reverse voltage across the relays. The load resistors are high power resistors meant to dissipate energy from the batteries as heat during discharge.

Temperature Measurement. The temperature measurement for each battery is taken on the outside skin in the middle of each battery. This measurement, as seen in Figure 14, is sent as a voltage value to a non-inverting OPAMP circuit. The relationship between measured temperature and the voltage value is $10\,mV\,/\,°C$ [27]. This OPAMP circuit buffers and amplifies, with a gain of 6, this voltage level. This signal is then sent via a 3 pin header back to the FPGA controller. Like the current measurement signal, this OPAMP circuit also filters the temperature measurement signal. Since the temperature measurement was expected to vary slowly in time, the corner frequency, as calculated with equation (2.14), was set for 30 Hz. This filter ensures that high

frequency noise is filtered out of the measurement. For this signal, the temperature sensor itself provides the galvanic isolation.

Temperature Measurement

Galvanic Isolation

+5 Volts from FPGA

Temp
Sensor

Temperature
Measurement to 8 bit AD
Converter and then to the
FPGA

10 kΩ

10 kΩ

3 Pin
Header

10 kΩ

50 kΩ

0.1 uF

0.1 uF
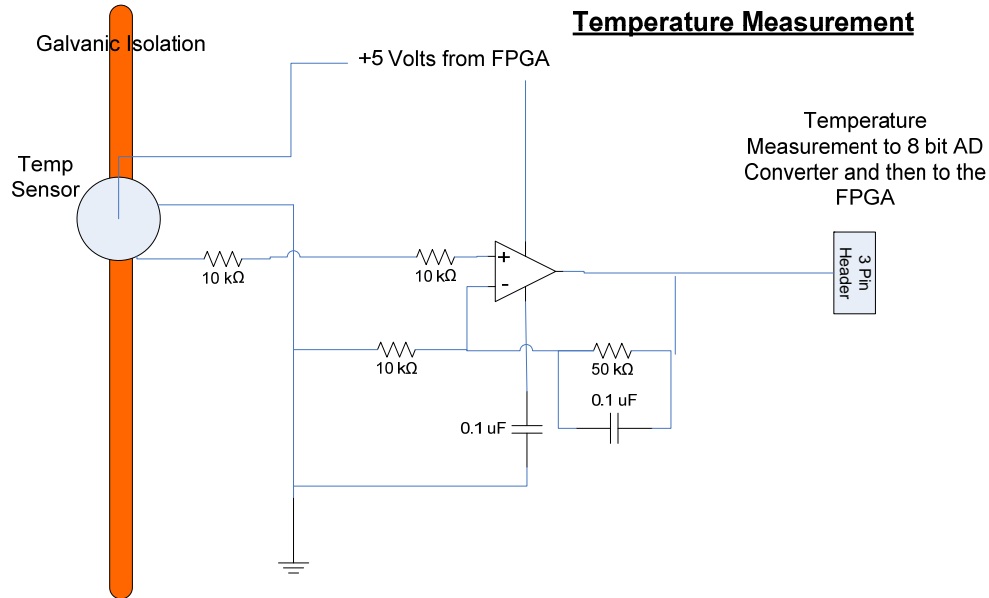
Figure 14.   Temperature Measurement Signal.

c.   *FPGA Controller Component*

The FPGA controller component including the software and hardware was created by Professor Alexander Julian at the Naval Postgraduate School. In general, it performs two functions for the pulse power system. These functions are to process the received signals sent to the controller and then to provide current and voltage control for the charger.

The signal processing conducted on the voltage measurement signal is to count the pulses, over a set period, of the square wave produced by the voltage to frequency converter. The signal processing for the current and temperature measurement is to convert these analog signals into 8-bit digital signals.

27

Although the control methodology used by the FPGA controller component will largely be discussed in the next section, the process of using a constant frequency to switch the converter MOSFET will be discussed here. This process, known as Pulse Width Modulation (PWM), is shown in Figure 15. This process uses a reference signal, shown as green in Figure 15, to compare to a constant frequency saw tooth waveform, shown as blue. When the reference signal is of a higher value than the saw tooth waveform, the FPGA controller would send out a "high" or "on" signal to the converter MOSFET switch. When the reference signal is of a lower value than the saw tooth waveform, the FPGA controller would send out a "low" or "off" signal to the converter MOSFET switch. The resulting signal from the constant comparison of the reference signal to the saw tooth waveform is shown as red in Figure 15. As can been seen in the figure, the PWM signal is a square wave signal of varying duty cycle that operates at the same frequency as that of the saw tooth waveform. Unless the reference signal were to exceed the maximum value of the saw tooth waveform or drop to zero, the PWM signal will continue operating at this same frequency [15], [16], [28].
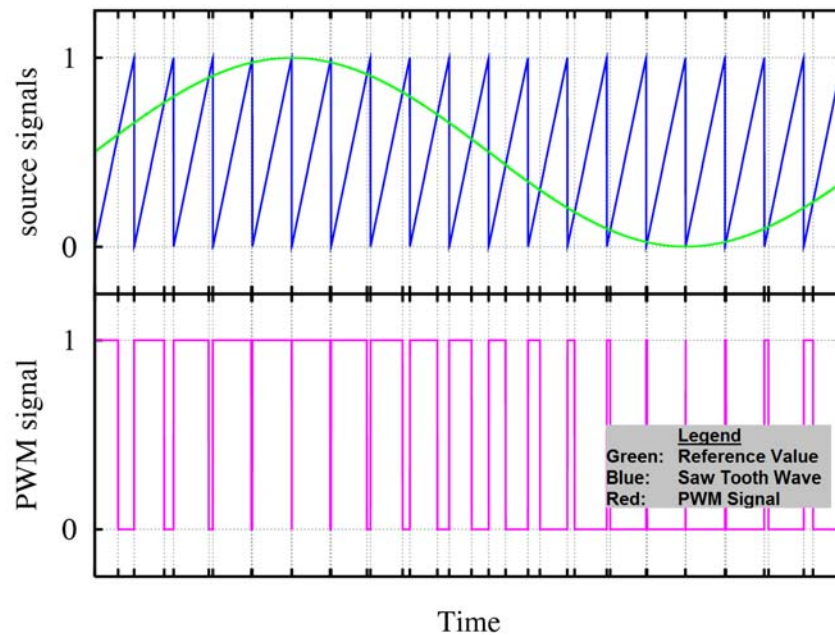
Figure 15.   Pulse Width Modulation. From [28].

28

d.   BMS Components Summary

The three components of the BMS system, the charger component, the power source and discharge component, and the FPGA controller component have been reviewed in the above section. Together, these components allow the BMS to perform its required functions: charging lithium-ion batteries, storing energy for the pulsed power application in lithium-ion batteries, and discharging the energy in pulses. The next section of this chapter will complete the discussion of the theory of operation of the BMS by using models of the BMS to demonstrate the charger control methodology.

C.   BMS CHARGING MODEL

1.   Overview

The BMS charging model is a combination of the models representing the buck converter, the controller, and the battery. Physically, the buck converter model represents the charger component, the controller model represents the FPGA controller component, and the battery model represents the energy storage part of the power source and discharge component. As such, the BMS model only simulates the CCCV charging process of the BMS. It does not simulate the pulse discharge of the batteries. The buck converter and controller models will be reviewed in the next section while the battery model will be briefly discussed. The entire BMS charging model and the associated MATLAB® code is shown in Appendix B.

2.   Buck Converter and Battery Models

The buck converter and the battery models are shown in Figure 16. The upper blue portion of this figure is the buck converter model. The lower orange section of this figure is the battery model.

The buck converter model simulates the two, first order differential equations necessary to describe a buck converter. These equations represent the current through the inductor of the converter and the voltage across the capacitor of the converter. These equations are not the more complicated equations seen as Equations (2.6) and (2.7) because the simulation represents the load as a full battery model instead of just a voltage source and inductance. The input to this buck converter in this simulation is a simple constant voltage, which represents the near constant voltage supplies to the charger by the smoothing capacitor, multiplied by the switching signal that is supplied by the controller model. As such, this converter model does not simulate the ripples in the current and voltage caused by the switching of the converter MOSFET.
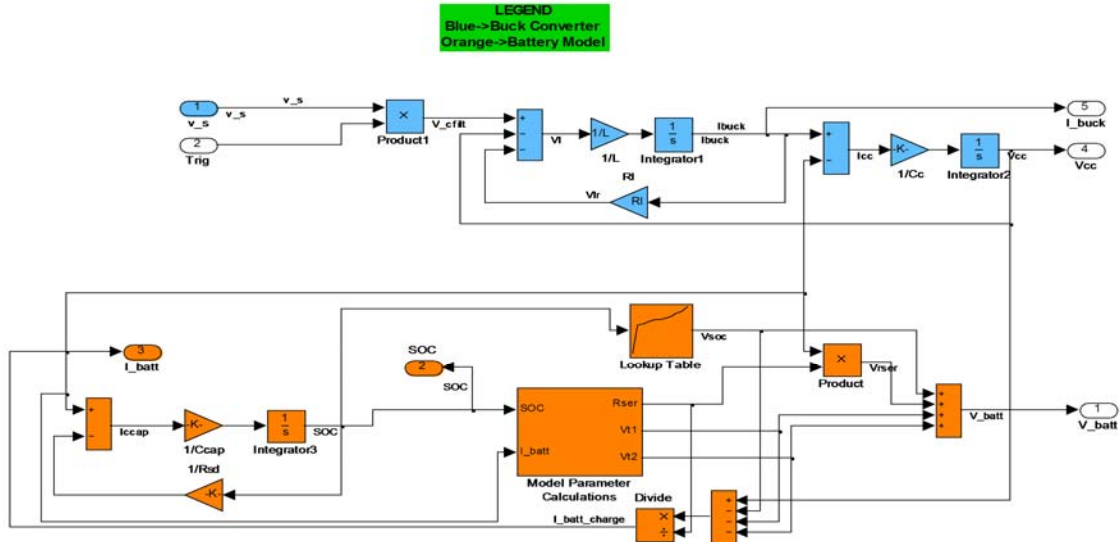
Figure 16.   Buck Converter and Battery Models.

An electrical model was chose as the load for the simulated buck converter. This model, presented in [29] and [30], uses various combinations of non-linear, equation-based resistors, capacitors, and inductors to model the charging of a commonly available commercial lithium-ion battery. The relevant charging specifications for this battery are listed in Table 5. During the operation of the model, lookup tables are used as the varying values for the electrical elements.

Battery Characteristic	Value
Capacity	850 mAh
CC Current Rating	0.80 A
CV Voltage Rating	4.10 V
Charge Cutoff Current (A)	10.0 mA

Table 5.   Battery Characteristics for the Battery Model.

3.   Controller Model

The model of the controller is shown in Figure 17. This model closes the inner current control loop and the outer voltage control loop. For the voltage control loop, this process is completed by subtracting the measured voltage at the converter capacitor from the CV voltage rating and then sending this value through a proportional–integral (PI) controller to create a reference current. For the current control loop, this process is completed by subtracting the measured current through the converter inductor from the reference current and then sending this value through another PI controller. The closing of the current control loop creates the duty cycle value that is sent to the MOSFET switch in the physical charger or to the multiplication block in the converter model. Saturation blocks are used at the output of each PI controller to ensure that the resulting values from these controllers are within suitable ranges. For the voltage PI controller, this range is from zero to the CC current rating. This saturation block ensures that the reference current never exceeds the CC current rating. For the current PI controller, this range is from zero to one. This ensures that the duty cycle is not less than 0% nor larger than 100%. A further limitation placed on the PI controllers is that each integrator is also given a saturation value. This value is the CC current rating for the voltage PI controller and one for the current PI

controller. These saturation values ensure that the integrators can quickly unwind from their summed values as the input values to the PI controllers grow smaller.
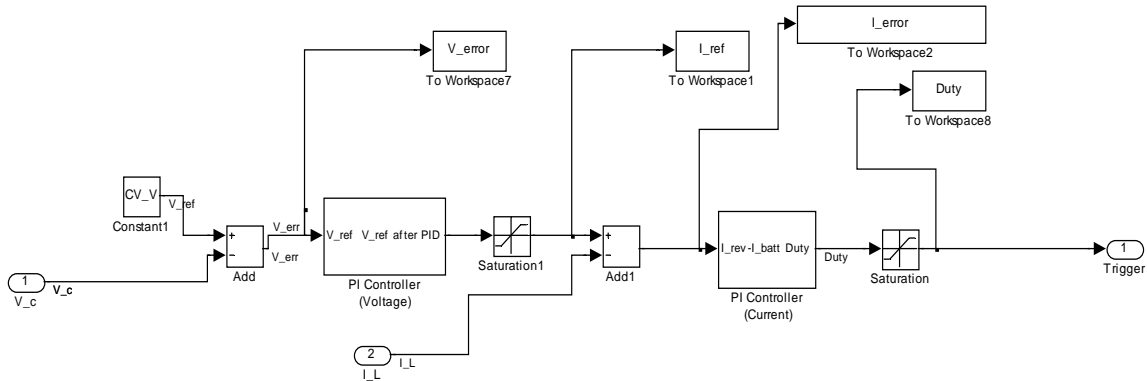
Figure 17.   Controller Model.

4.   Model Results

The model results were obtained with the PI controller gains as listed in Table 6. These gains are higher than would be necessary for the physical system but were necessary for the short duration of the simulations. These high gains ensured that the steady state current and voltage values of the converter were reached quickly enough to see during the short simulations.

Each simulation run produces voltage and current versus the state of charge of the battery waveforms. Only the last 50% of data from both the current and voltage waveforms were kept from each simulation run. This is another measure to ensure only the steady state values of each simulation are observed.

The model results were produced by running the simulation repeated at approximately every 2% battery state of charge as the initial starting condition. These individual simulation results were then combined and plotted as the result.

Controller Gain Description	Gain Values
Current Proportional Gain	1.5
Current Integral Gain	1.9
Voltage Proportional Gain	1.4
Voltage Integral Gain	3

Table 6.   PI Controllers' Gains.

The results of a typical charging profile is seen in Figure 18. The results show the current and voltage charge curves from approximately 5% battery state of charge to 100% battery state of charge. Figure 19 shows a closer view of the transition from the CC to the CV stages of charging. As can be seen, the battery stays in the CC stage up to approximately 92%. As seen from the data strips, the CC charge stage produces the desired 0.80 A charging current. Also during this time, the voltage is slowing increasing up to the limiting value of the CV voltage rating. At approximately 92%, the stages change from CC to CV. At this point, the CV voltage rating of 4.1 V is reached and then maintained. At the same time, the current begins to drop as the voltage level is maintained. Figures 18 and 19 show that this model of the BMS is correctly executing the CCCV charging process.
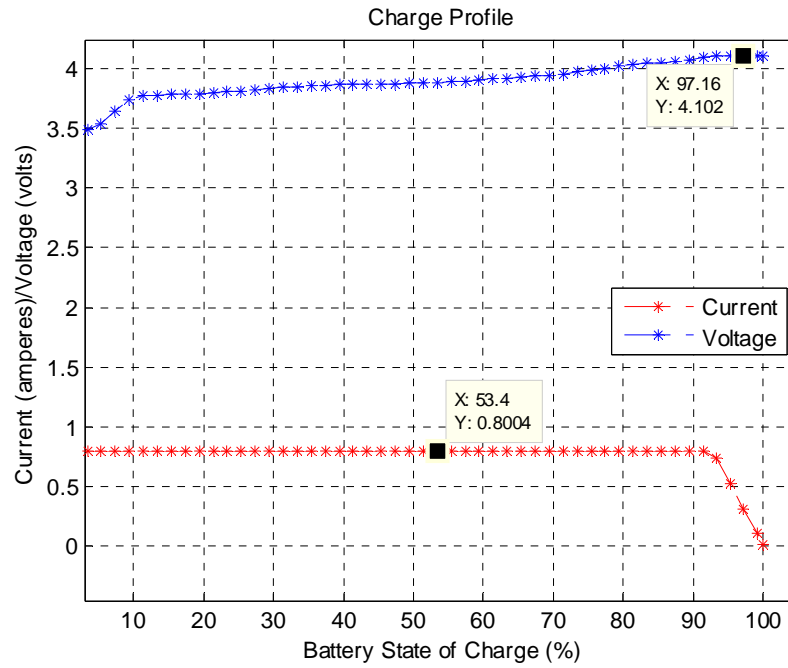
Figure 18.　Typical Charge Profile.
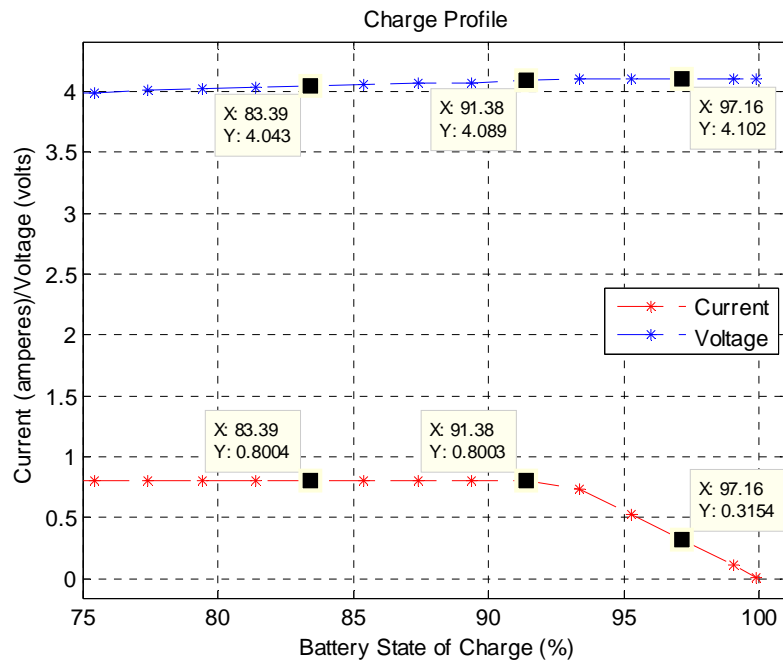
Figure 19.　Transition Point from CC to CV Stages.

34

D.   CHAPTER SUMMARY

This chapter has reviewed the functions that the BMS must perform to accomplish the requirements of a pulsed power system. It has also explained the components and parts of the BMS that allow it to perform these functions. Finally, the theory of operation of the BMS has been discussed through the explanation of its functions and through the explanation of the BMS charging model. The next chapter will review the process of building the actual BMS.

THIS PAGE INTENTIONALLY LEFT BLANK

III.   CONSTRUCTION AND TESTING OF THE BMS

A.   OVERVIEW

The previous chapter dealt with the design and theory of operation of the BMS. This following chapter will review the process of turning this design into a physical system. The steps taken to complete this construction and assembly process are shown in the following list. These steps will be discussed under the three topics of hardware, software, and testing.

- Construction of the safety features.

- Design and construction of the charger PCB.

- Design and construction of the FPGA controller software and PCB.

- Assembly of the physical BMS.

- Testing of the charger PCB and BMS charging and discharging capabilities.

Before discussing the creation of the BMS, the system capabilities will be reviewed. The BMS capabilities can be explained by only a few characteristics including its maximum charging current, its maximum charging voltage, and its maximum discharge current. While other characteristics could be listed to help understand the capabilities of this pulsed power system, these three items are the most important to understand the capabilities and limitations of the BMS. These capabilities and the features limiting them are listed in Table 7 [21], [31], [32], [33].

Capability Description	Value	Limiting Feature
Maximum Charging Current	10 A	Converter MOSFET Switch
Maximum Charging Voltage	4.5 V	Saturation of the OPAMP Amplifier for the Current Measurement Signal and Saturation of the Voltage to Frequency Converter
Maximum Discharge Current	240 A	Discharge Switch

Table 7.   BMS Capabilities and Limiting Features.

B.   HARDWARE

1.   Safety Features

Several safety features were built into the design of the BMS. The first safety feature is an emergency stop switch, seen as the red button in the bottom left corner of Figure 20, stops the flow of energy to the charger system. The next safety feature is the Plexiglas enclosure, also seen in the same figure, surrounding the entire BMS. This enclosure includes a fan that vents the air from the BMS to the outside of the building. This feature was necessary in order to vent fumes in the case of a lithium-ion battery rupture or explosion. Appendix A lists the safe operating procedures for the BMS and covers the use of these safety features in more detail.
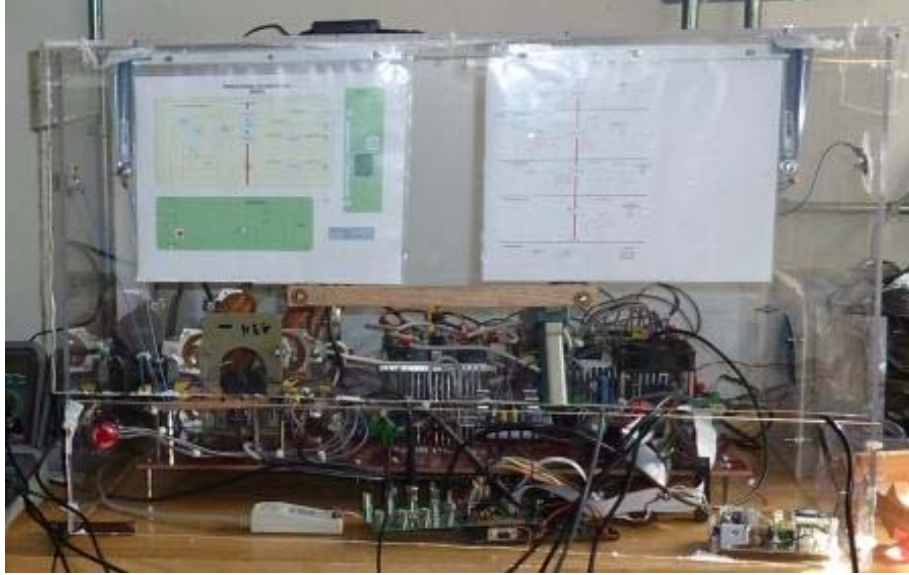
Figure 20.   BMS Safety Features.

2.   Charger Component PCB

The construction of the charger component PCB began with the creation of the PCB schematic and layout. These electronic documents were then used by a commercial vendor to produce the PCB. This PCB, without attached parts, is seen in Figure 21. The red line divides the PCB into two sections: the signals section, below the red line and the charger section, above the red line.
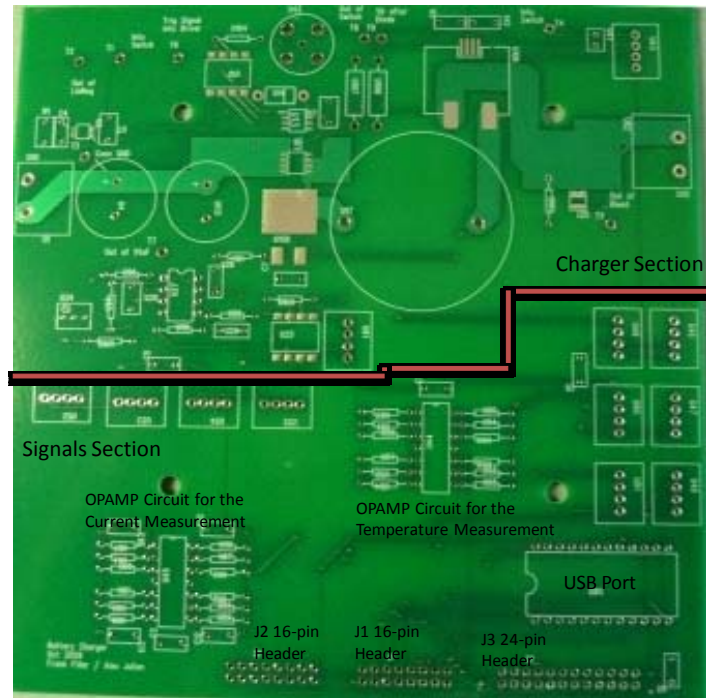
Figure 21.   Blank Charge Component PCB.

The signals section, which is only filled with parts on one of the charger component PCBs, collects and routes all of the measurement signals from all of the batteries and charger components to the single FPGA controller board. In addition, the signals section contains all of the OPAMP circuits that buffer, amplify, and filter the current and temperature signals from all four chargers. Further, the signals section contains a USB port that routes signals from the FPGA controller board to the computer. Additionally, the signals section routes the discharge signal from the FPGA controller to the discharge switches on the power source and discharge component. Finally, the signals section routes 5 V power to several components on the charger component PCB.   The signals section performs this signal routing function from the one charger component PCB to the FPGA board via two 16-pin header and one 24-pin connectors.

The pin layouts for these header connectors are listed in Table 8. Figure 21 shows the locations of the major parts of the signals section. The following list is a summary of the functions performed by the signals section of the charger component PCB.

- Collects and routes all of the voltage measurement signals from the four chargers to the FPGA controller board.

- Collects, amplifies, and routes all of the current measurement signals from the four chargers to the FPGA controller board.

- Collects, amplifies, and routes all of the temperature measurement signals from the temperature sensors on the four batteries to the FPGA controller board.

- Routes the USB signals from the FPGA controller to the computer.

- Provides a 5 V power source to components on the charger component PCB to include the voltage measurement signal optocoupler, the Hall Effect sensor, and the temperature sensor.

Pin #	Signals Type on each Connector		
	J3	J2	J1
1	GND	V1	USB pin 1
2	GND	GND	GND
3	I1	V2	USB pin 2
4	GND	GND	GND
5	I2	V3	USB pin 3
6	GND	GND	GND
7	I3	V4	USB pin 5
8	GND	GND	GND
9	I4	NC	USB pin 8
10	GND	GND	GND
11	T1	NC	USB pin 10
12	GND	GND	GND
13	T2	USB pin 22	USB pin 12
14	GND	GND	GND
15	T3	USB pin 23	USB pin 18
16	GND	GND	GND
17	T4	-	-
18	GND	-	-
19	NC	-	-
20	GND	-	-
21	NC	-	-
22	GND	-	-
23	5 V	-	-
24	GND	-	-
Legend			
V#: Voltage Measurement from Charger #			
I#: Current Measurement from Charger #			
T#: Temperature Measurement from Battery #			
USB pin #: Signal to a Pin on the USB Port			

Table 8.   Pin Assignments for the 16-pin and 24-pin Header Connectors.

The charger section is for mounting all of the parts of the buck converter as well as the parts necessary for the voltage measurement signal and the current measurement signal up to the point before it is amplified.

The one charger component PCB with both the charger section and the signals section filled with parts is shown in Figure 22. Major parts are labeled in this figure. For comparison, a charger component PCB without the signal section parts attached, is shown in Figure 23.
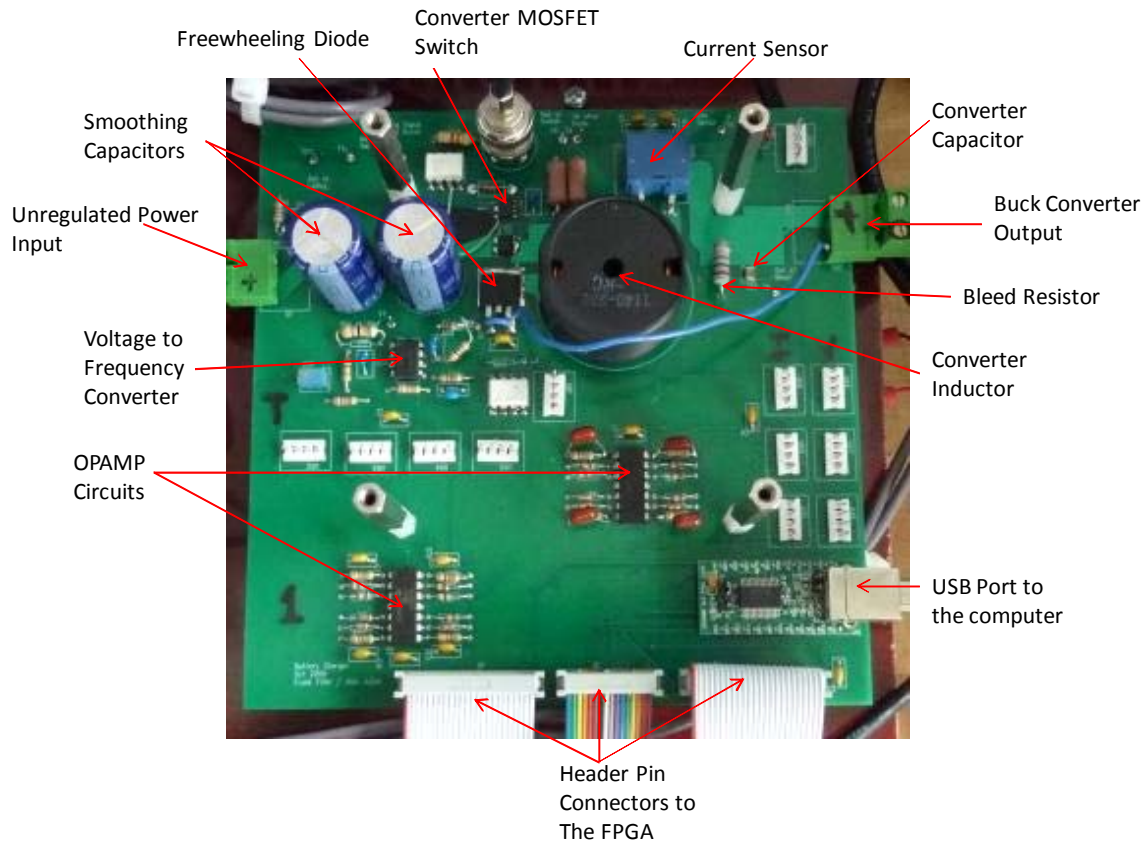
Figure 22.   Charger Component PCB with the Charger and Signals Section Completed.

Figure 23.   Charger Component PCB with only the Charge Section Completed.

Each of the charger component PCBs was created with several test points in order to aid in troubleshooting problems with the board. These test points and the signals they are sampling are shown in Table 9.

Test Point #	Signal Measured
1	Voltage into the MOSFET Switch
2	Voltage Provided by the Linear Regulator
3	Ground of the Buck Converter (At the Linear Regulator)
4	Output of the Current Sensor before Amplification
5	Ground of the Buck Convert (At the Bleed Resistor)
6	Switching Signal into the MOSFET Driver
7	Voltage out of the Voltage to Frequency Converter
8	Voltage after the MOSFET Switch
9	MOSFET Driver Bootstrap Voltage

Table 9.   Charger Component PCB Test Points.

3.   FPGA Controller Hardware

The hardware for the FPGA controller was designed by Professor Alexander Julian at the Naval Postgraduate School. This hardware includes the FPGA board, an adapter board, and a power supply. This hardware can be seen in Figure 26.

4.   BMS Assembly

With four charger component PCBs and the FPGA controller component assembled, the remainder of the BMS can be constructed. The only component of the BMS yet to be discussed is the power source and discharge component. The parts of this last component, as well as the other components, were assembled onto a single piece of Phenolic. The completed BMS with important parts labeled is shown in Figure 24.
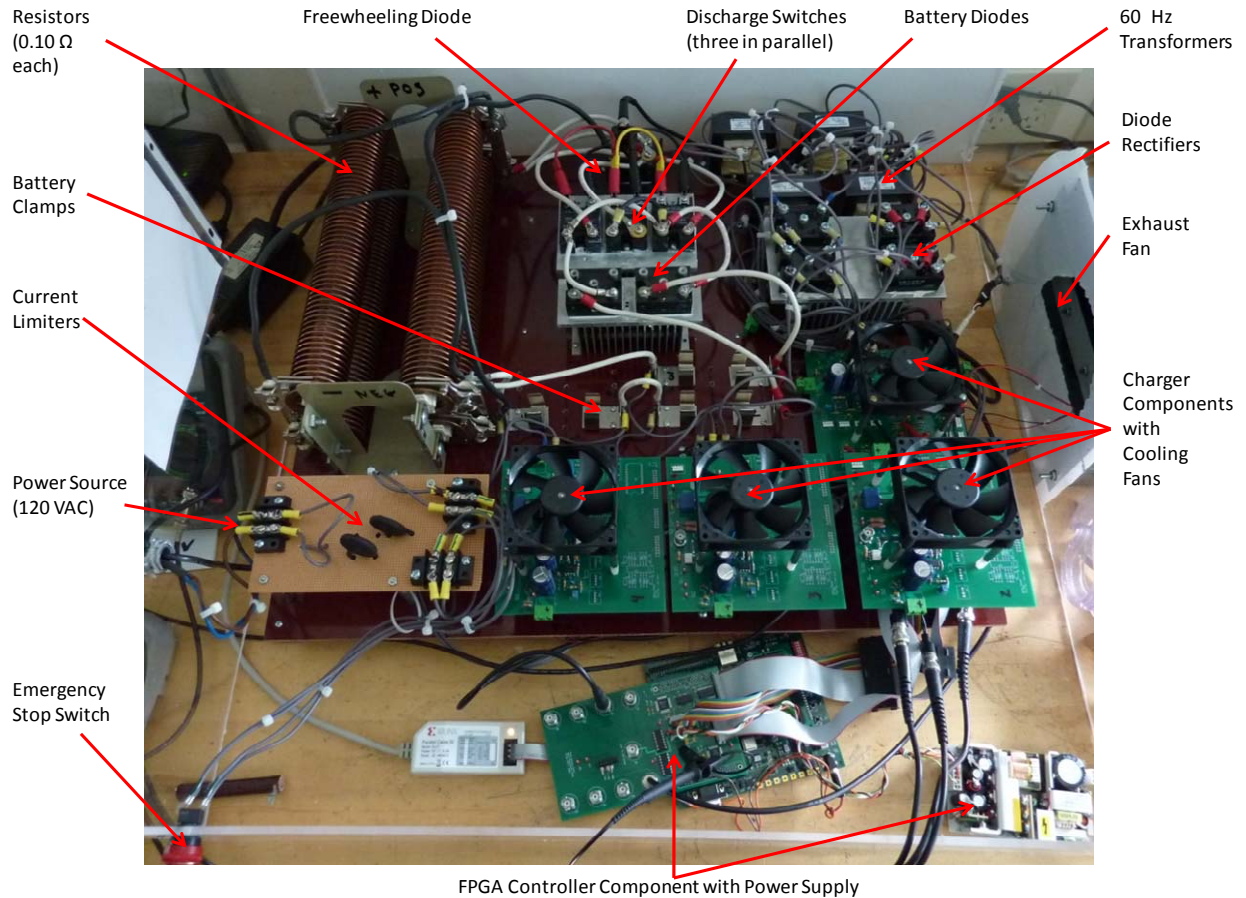
Figure 24.   Assembled BMS.

Two other aspects of the BMS construction are worth discussing. The first aspect is thermal management. Several parts of the BMS had the potential to become very hot during operation. These include the converter MOSFET switch, the diode rectifiers, the discharge MOSFET switch, the diodes in series with the batteries, and the freewheeling diode in the discharge path. To cool the converter MOSFET switches, 80 mm, 12 V fans were installed on each of the charger component PCBs. These were operational whenever the charger was operational. To cool the other parts mentioned, each was attached to a heat sink with a thermal compound used to seal the connection. The thermal management measures can be seen in Figure 24. The second consideration was the inductive energy stored in the discharge path. Even with the freewheeling diode, the potential of damaging the discharge switches with high reverse voltages was

46

significant. In order to reduce the inductance in this discharge path, all of the wiring connecting the discharge switches to the freewheeling diodes and to the resistors was minimized. Although difficult to see in Figure 24, these components were placed as close as possible to each other to minimize the wiring between them.

C.   SOFTWARE

The software that controls the CCCV charging process in the FPGA was designed by Professor Alexander Julian at the Naval Postgraduate School. It is similar in execution but more robust in capabilities than the controller model explained in Chapter II.

D.   TEST PLAN

1.   Introduction

Upon completion of the BMS construction, a test plan was followed to confirm the correct functioning of the BMS. The test plan ensured that the BMS could perform its intended functions and that the data received as measurements from the system provided relevant information. The following test plan is discussed next.

2.   Test Procedures

Most of the following procedures were accomplished during the testing of the charger component PCBs and the overall BMS. If an unexpected result or an otherwise failed test occurred, troubleshooting began until the problem had been satisfactorily explained or the problem resolved.

- Test the emergency stop switch to ensure no power was passed to the BMS when the switch is opened.
- Test the switches on the buck converters to ensure they did not pass power through when in an open position.
- Test the discharge switches to ensure they did not pass power through in an open position.

- Take measurements at each of the test points on the chargers to ensure measured values were as expected.

- Sample the current, voltage, and temperature measurements returned by the BMS to ensure they were as expected.

- Test the BMS on one battery at a low charge and discharge current. Ensure the BMS performed as expected.

- Test the BMS on multiple batteries in series. Ensure the BMS performed as expected.

- Test the BMS on multiple batteries in series strings that are in parallel. Ensure the BMS performed as expected.

3. Results of the Test Procedures

The following problems were noted and corrected during the testing procedures.

a. *Charger Component PCB*

Several changes were required to the charger component PCB due to design flaws in the circuit layout and to improve the quality of signals received from this board. The changes are shown in the following list.

- A 1.5 kΩ resistor connected the 5 V source of the FPGA to the Vcc terminal of the voltage measurement optocoupler on the designed PCB. Both the connection points and the value of the resistor were modified. The correct value of this resistor was 200 Ω and should have been connected from the Vout terminal of the optocoupler to the 3 pin header. To correct this design error, the 200 Ω resistor was not mounted in the through-holes designed for this part, but was instead directly soldered from the Vout terminal of the optocoupler to the 3 pin header.

- Significant copper was left on the PCB for the primary path of the charging current in order to reduce the current density and therefore heat generation in this current path. This concept was correctly applied to the PCB in the

necessary areas except from the anode of the converter freewheeling diode to the converter ground path. This path was mistakenly not increased in width to account for the return path of the charging current. To correct this error, a wire was soldered from the anode of the diode to the ground pin of the charge current output terminal.

- The reset pin of the MOSFET driver was connected to the input pin of the driver in the PCB design. The correct connection is to connect the reset pin to the output of the optocoupler. This change sends the switching signal through the reset pin. To accomplish this correction, the surface connection between reset pin and the input pin was cut and then a wire was soldered between the output of the optocoupler providing the switching signal and the reset pin of the MOSFET driver. In addition, the input pin of the driver was initially connected to the output pin of the optocoupler. It was carrying the switching signal in the original, incorrect PCB design. To correct this error, the surface wire connecting the optocoupler and the input pin were cut and a wire was soldered from the input pin to ground. The reason the reset pin was used as the switching pin for the driver was due to the active low input logic of this driver for the input pin.

- The resistor that connected the 5 V linear regulator source to the input or anode of the voltage measurement optocoupler was designed to be 10 kΩ in order to limit the current into optocoupler. Unfortunately, this resistance did not allow enough current into the optocoupler in order to operate this device. Instead, a 2 kΩ resistor was inserted in place of the original resistor.

- When the current measurement signal from the charger component PCB to the FPGA was initially tested, the signal revealed significant high frequency ripple. In order to reduce this problem, and per the earlier discussion about the filter capabilities of the OPAMP circuits, a capacitor with a value of 80 nF was added in parallel with the feedback resistor to provide a cutoff frequency

of 2 kHz. This additional capacitor significantly decreased the high frequency ripple of the current measurement but was not part of the original OPAMP circuit design.

- Initially, the voltage to frequency converter was not functioning beyond input voltages over approximately 3.8 V. Since the Vcc value for this device was 5 V, this shut down was determined to be the saturation of the comparator portion of the voltage to frequency converter [21]. To correct this problem, a voltage divider network was added to the input to the voltage to frequency converter to lower the input voltage to $\frac{3}{4}$ of the original value. This ratio ensured that the maximum charging voltage of 4.5 V was seen as approximately 3.4 V by the voltage to frequency converter. This lowered voltage level prevented the comparator from saturating.

- The resistor on the switching signal input from the FPGA was intended to limit the current input to the optocoupler on this signal from a 5 V signal. Instead, the input signal was actually provided at 15 V. To correct this error, the input resistor was increased from 1 $k\Omega$ to 4.5 $k\Omega$.

- When the voltage measurement out of the voltage to frequency converter was initially tested, it contained too much noise to be useful. To reduce this noise, the capacitor from the input of the voltage to frequency converter to ground was increased from 0.1 μF to 1 μF. This increase still kept this capacitor within the recommended range of this device as recommended in [21].

- The linear regulator requires a minimum load to produce at least 1 mA of current in order for the regulator to correctly provide a constant 5 V. As an operational precaution to ensure that this load condition always exists, a 2 $k\Omega$ load was added to the voltage output pin to ground of the regulator.

b.   *Power Supply and Discharge Component*

Only one change was required on the power supply and discharge component. Initial charge testing of batteries revealed the existence of a large ripple at the switching frequency, 30 kHz, in the charge current. This ripple, seen in Figure 25, is approximately 4.5 A peak-to-peak while in the CC stage of charging at 1 A.   This value is far too high and would have resulted in unnecessary heat buildup in the charged batteries. In order to reduce this ripple, a 9.7 uH inductor was added in series to the battery in the charging path. This inductor significantly reduced the ripple as seen in Figure 26. Although the 30 kHz ripple is difficult to determine in this figure, it is approximately 1 to 2 A peak-to-peak while charging in the CC stage at 5 A. This ripple is a much lower ripple value and a much lower percentage of the charging current.
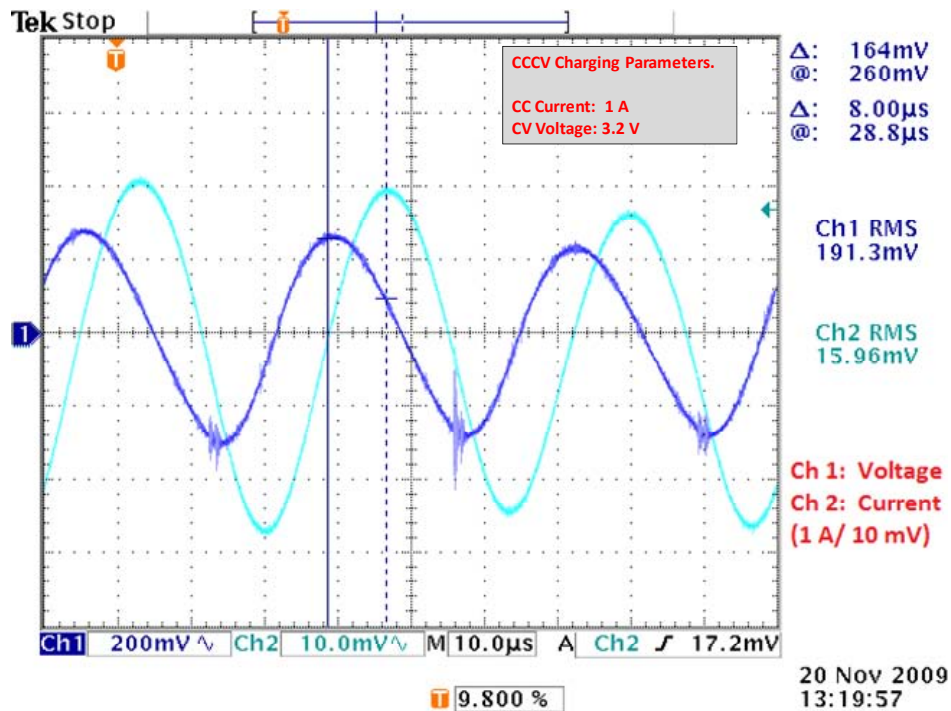
Figure 25.   Initial Charge Current Ripple (AC Coupled).
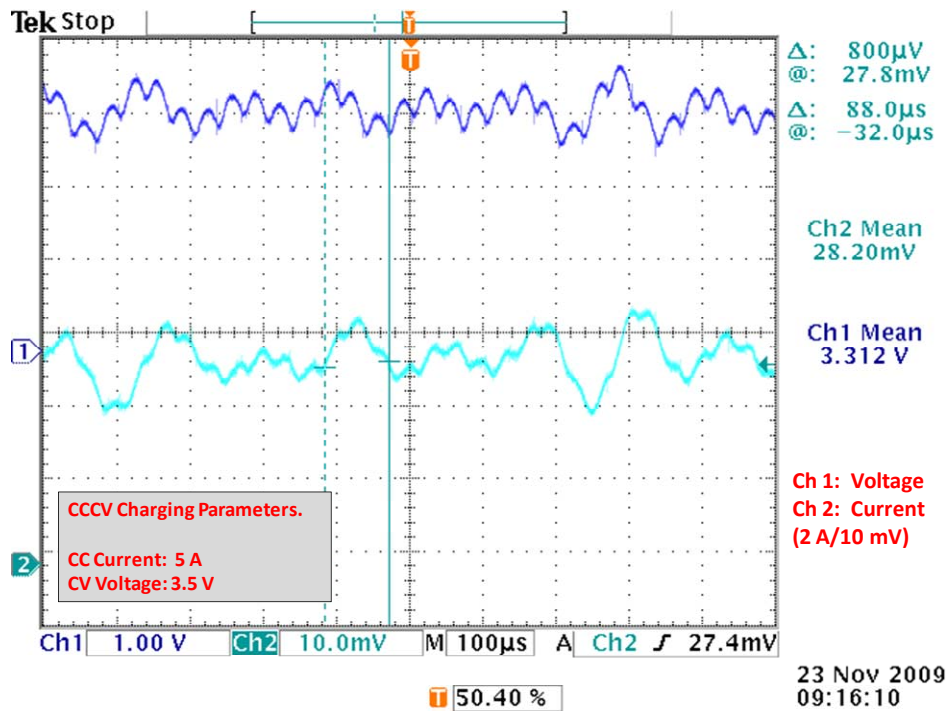
Figure 26.   Charge Current Ripple after Inductor Addition (DC Coupled).

E.   CHAPTER SUMMARY

This chapter has reviewed the construction, assembly, and testing of the BMS.   Details of the charger component PCB construction and assembly considerations during the construction of the BMS have been covered.   The testing plan for the BMS and the associated results have been presented. Finally, the numerous modifications to the BMS, especially the charger component PCB, have been detailed.   The next chapter will review the results of multiple charging and discharging cycles and determine the functionality of the BMS.

IV. RESULTS AND CONCLUSIONS

A. OVERVIEW

The data presented in this chapter are the results of tests meant to confirm that the BMS was capable of charging lithium-ion batteries by using the CCCV process and then discharging them using repeated pulses. The results are used to confirm the operation of the BMS as a viable design to the pulse power system requirements identified in the introduction. Although the results indicate the BMS is capable of meeting the identified requirements, the BMS was not tested at its full capabilities due to time restrictions. These results represent the charging and discharging of a single commercially available lithium-ion battery, with the characteristics as listed in Table 10. In addition, these results were conducted at charge voltages and charge and discharge currents below the maximum capabilities of the BMS as identified previously. Additional testing of this system is one of the recommendations made in the "further research" section of this chapter.

Battery Characteristic (Units)	Value
Capacity (A-hr)	4.4
Maximum Continuous Discharge Current (A)	136
CC Current Rating (A)	40
CV Voltage Rating (V)	3.6
Charge Cutoff Current (A)	0.40
Discharge Cutoff Voltage (V)	2.5

Table 10. Battery Characteristics of the Test Battery.

B.   RESULTS

As discussed in the testing section of Chapter III, the initial testing of the BMS resulted in very large current ripples through the battery. The plot of the current ripple through the battery during these initial tests is shown again in Figure 27. An important note is that this oscilloscope plot was generated while AC coupled so no DC values are present. In addition, the ripples in Figure 27 have a frequency of 30 kHz that is caused by switching frequency of the converter switch. This plot allowed the calculation of impedance of this battery by comparing the RMS values of the voltage and current waveforms and by measuring the angle between the peaks of these waveforms [16], [23]. Using this method, the impedance for the test battery was determined to be $0.120\angle - 86.4^{\circ}\ \Omega$ or $7.5\times10^{-3} - j120\times10^{-3}\ \Omega$. This is almost purely inductive which accounts for the large current ripple generated when charging this battery.
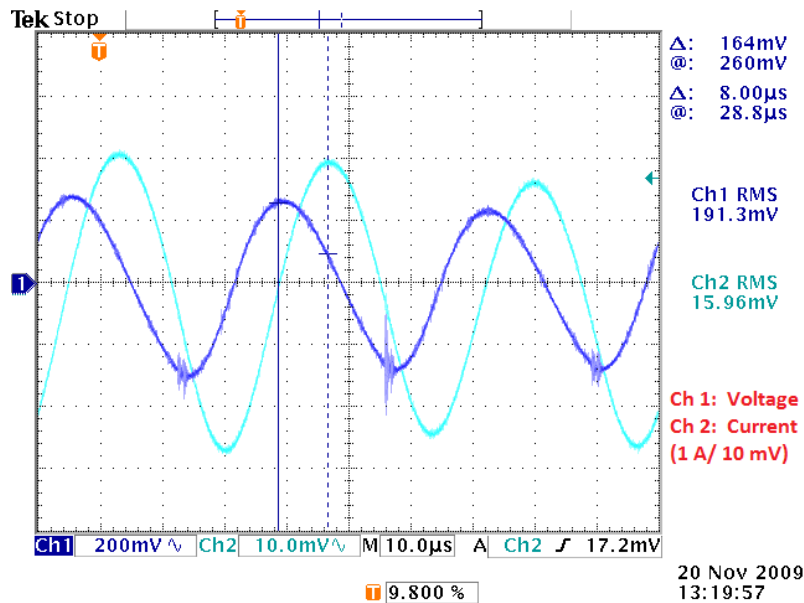
Figure 27.   Initial Charging Tests before Adding the Series Inductance (AC Coupled).

Also as discussed, a 9.7 uH inductor was added in series with the battery in order to reduce this current ripple. The results presented were generated with this added inductor.

Two charge and discharge cycles are shown in the following figures. One data set is shown in Figures 28 and 29. A second data set is shown in Figures 30 and 31. Both charging and discharging cycles had the same CV voltage values of 3.5 V, but the first cycle had a CC current value of 4 A and a discharge resistance of 0.05 Ω while the second cycle had a CC current value of 5 A and a discharge resistance of 0.025 Ω. Figures 28 and 30, the charge and discharge curves, show the temperature, current, and voltage values as measured by BMS sensors. Figures 29 and 31, the discharge curves, show the voltages and currents of the discharge processes as measured directly at the battery and displayed on an oscilloscope.
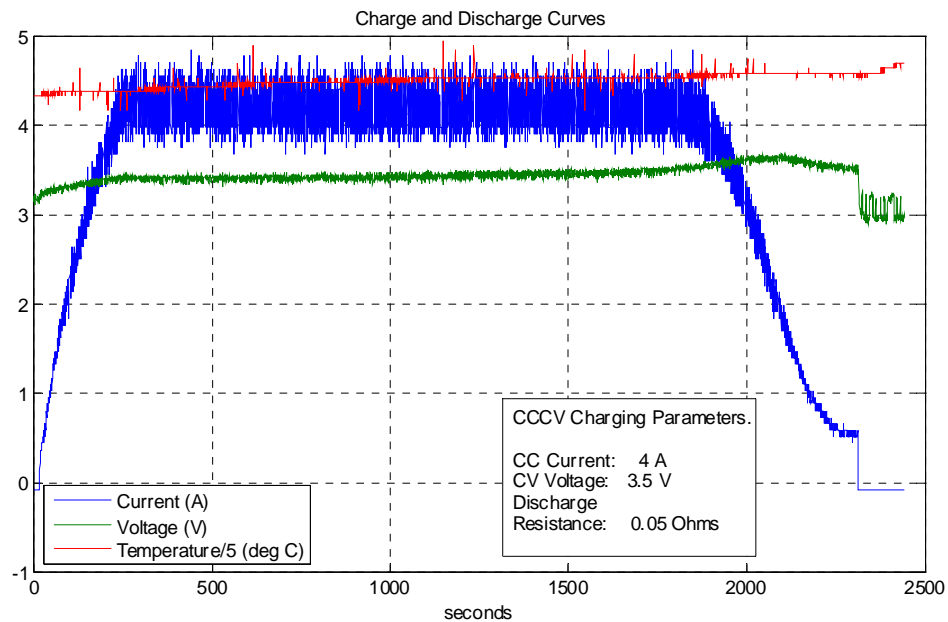
Figure 28.   Charge and Discharge Curve, First Data Set.
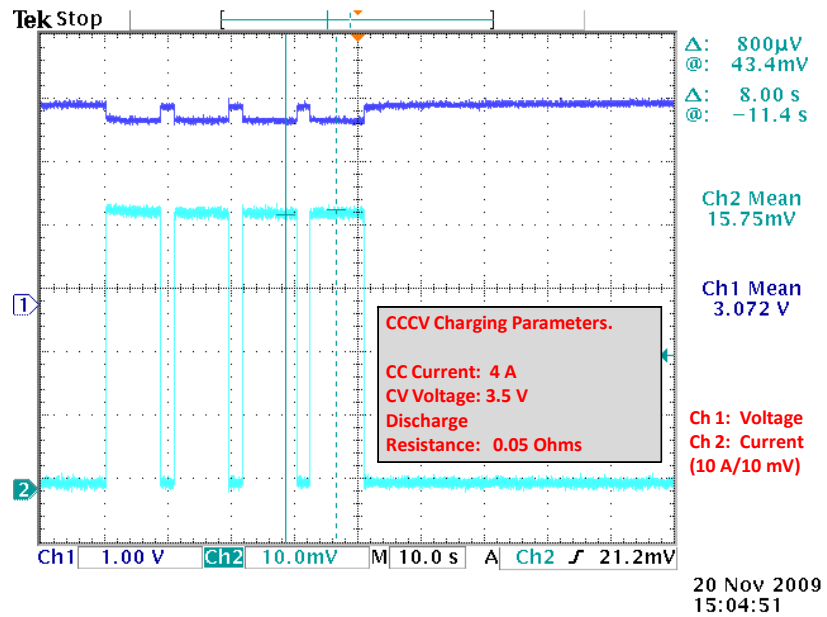
Figure 29.   Discharge Curve, First Data Set.
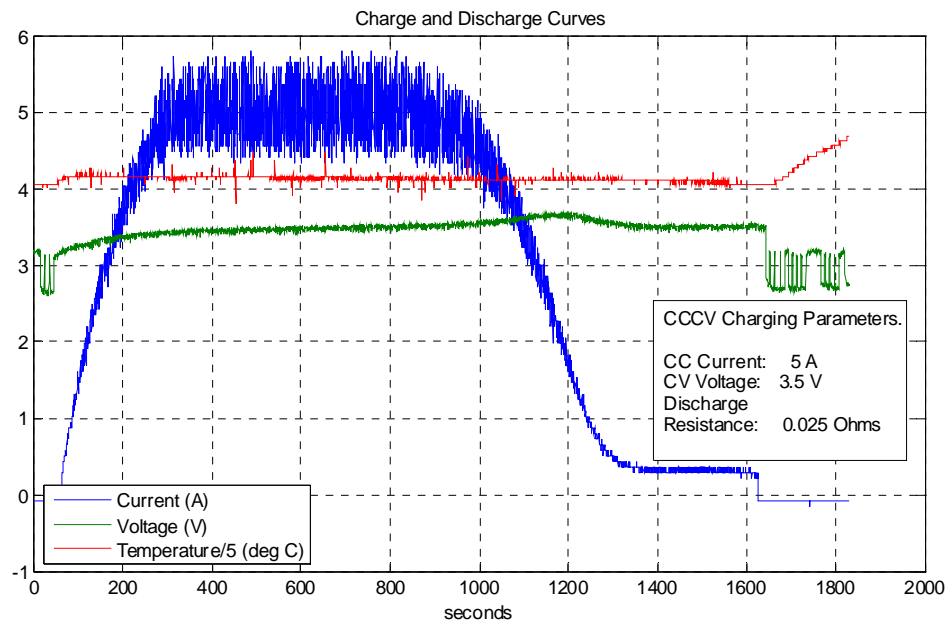
Figure 30.   Charge and Discharge Curve, Second Data Set.
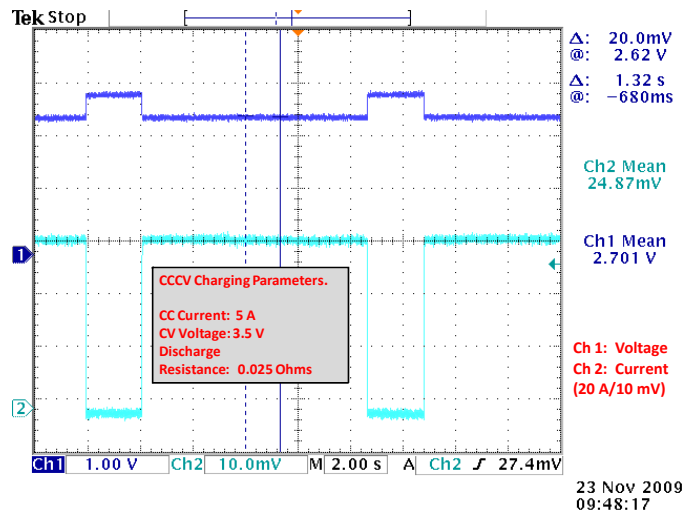
Figure 31.   Discharge Curve, Second Data Set.

Both data sets support the following conclusions:

- The BMS successfully charges the battery using the CCCV charging process. In both data sets, a constant current stage is reached as shown by the limiting current values reached on each plot. Also in both data sets, a constant voltage stage is reached as shown by the limiting voltage values reached on each plot. The transition point between these two stages of the CCCV charging process, is shown in more detail using the data from the second data sets in Figure 32. As can be seen, the voltage does slightly overshoot the desired CV voltage value, but then settles back to the correct value of 3.5 V. The current, as the charging process is coming out of the CC stage to the CV stage appropriately begins slowly decreasing in value.
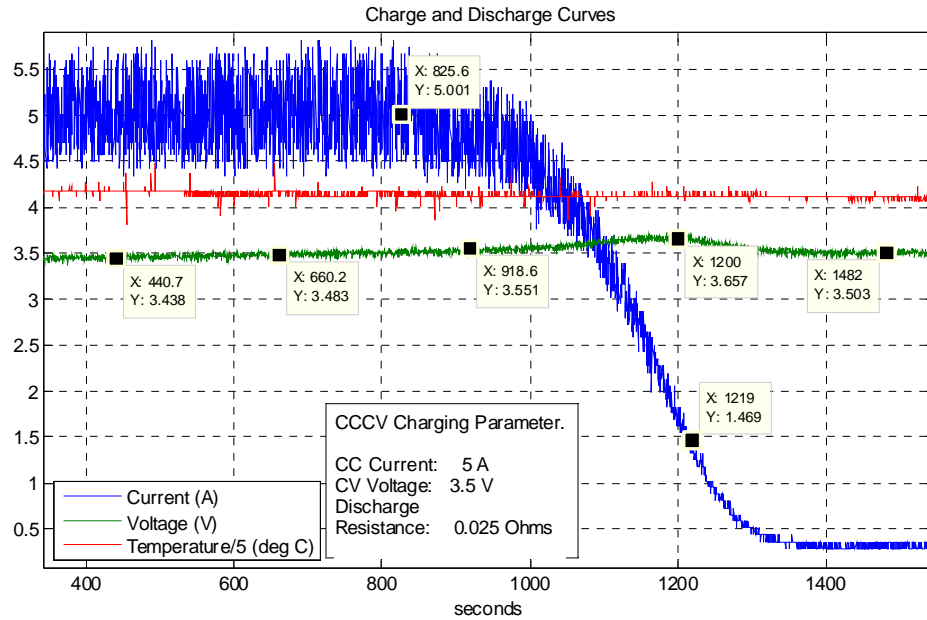
Figure 32.   CC to CV Transition, Second Data Set.

- Figures 29 and 31 show the current and voltage levels of the battery during discharge. The plots show the pulsed release of energy from this battery at currents of approximately 42 A for the first data set and 64 A for the second data set. Also shown on these plots, as well as Figures 28 and 30, are the expected voltage sags during high current discharges [34], [35], [36].

- Finally, Figures 28, 30, and 33 show the expected temperature rise during pulse discharges of the battery [34], [35], [36]. As seen in Figure 33, the temperature of the battery in the second data set rises from approximately 20.3 $°C$ to 23.4 $°C$. This rise in temperature was over 12 pulses of 2 seconds duration each.
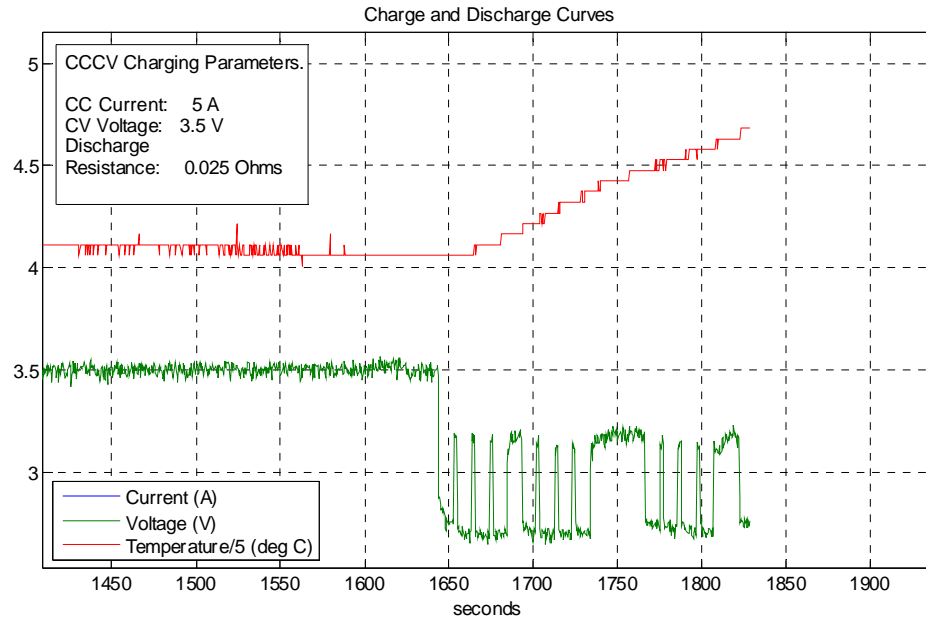
Figure 33.   Temperature Rise of the Battery in the Second Data Set.

C.   RECOMMENDED FURTHER RESEARCH

While the results of the one-battery charge and discharge process indicated that the BMS successfully meets the requirements of the pulse power system, further testing of this system and improvements to the system are possible. The following list indicates the recommended areas of further research.

- Testing the BMS with two parallel strings of two batteries.

- Testing the full charge and discharge capabilities of the BMS.

- Miniaturize the chargers to make this a more economical and viable design. This process can be accomplished by the research and construction of other charger topologies.

- Create the software for and test the BMS using different charging processes.

- Create the software for and test the BMS with other types of batteries.

## D.	CHAPTER SUMMARY

Results of two charging and discharging cycles have been presented in this chapter. The results indicated that the intent of the BMS, to provide the capabilities of a pulse power system, has been achieved. These results, though, are preliminary and should be further supported with additional testing of the BMS. Further, the BMS begins to establish a battery research capability at the Naval Postgraduate School. The BMS should be a flexible battery charging system that can be modified for different charging processes or different batteries with only a software change.

APPENDIX A. BMS SAFETY PROCEDURES

1. <u>Summary</u>. This document is meant only to summarize safety procedures for the battery experiments conducted in the NPS power laboratory. It is not meant to be comprehensive safety standard operating procedures for battery experiments.

2. <u>References</u>. Information in this document was gathered primarily from the Material Safety Data Sheets for the commercially available batteries to be used in the BMS. In addition, information from the Lawrence Livermore National Laboratory Safety Notice, "Solid-State Heat-Capacity-Laser (SSHCL) Lithium-Ion Battery System" was used in this document [37].

3. <u>Dangers</u>. All lithium-ion batteries can either explode or catch on fire from the following circumstances. Steps to mitigate the occurrence of these circumstances, whenever possible, will be taken before conducting any battery experiments.

    a. External or internal battery shorts.

    b. Overcharging.

    c. Excessive current during discharging or charging.

    d. Over discharging.

4. <u>Requirements for Experimentation</u>.

    a. All charging and discharging activities will be physically monitored by personnel in the laboratory. At no time will these activities be left unattended.

b. <u>Physical Safety Precautions</u>.

    i. In order to lessen the dangers from a potential battery explosion, a Plexiglas or similar material covering will fully enclose the batteries in the BMS. This covering will be in place during any charging or discharging activities.

    ii. The BMS will have a physical kill switch that removes all energy sources from the batteries. In addition, the BMS will have a physical kill switch that removes all energy sources from test loads. These switches should be located outside protective cover.

    iii. The protective covering for the batteries will be vented using a fan to draw air out of the enclosure to the outside air. This ventilation system will be active during all charging or discharging procedures. This system will remove harmful fumes in the case of a battery fire.

c. <u>Safety Equipment</u>.

    i. The following safety equipment will be in the vicinity of the BMS at all times:

        1. Safety apron.

        2. Safety gloves.

        3. Goggles.

        4. Fire extinguishers.

            a. Type ABC for use on cells that have not ruptured.

            b. Type D fire extinguisher for use on cells that have ruptured.

d. <u>Handling</u>.

   i. <u>Intact Batteries</u>. No special safety precautions are necessary when handling intact batteries except those necessary to prevent accidental discharge.

   ii. <u>Ruptured Batteries</u>. Ruptured batteries will only be handled by individuals with the appropriate personal protective equipment-safety gloves, safety apron, and eye protection. These batteries should be appropriately disposed of.

5. <u>Responses to accidents</u>.

   a. <u>Ruptured Batteries</u>. Ruptured batteries may be safely disposed of by individuals wearing the above listed protective equipment. Any materials that have either leaked out of the batteries or exploded out of the batteries will be cleaned up with absorbent material and then disposed of.

   b. <u>Battery Fires</u>. Laboratory personnel will not try to fight a battery fire unless it is necessary for the safe escape of personnel.

6. <u>Storage</u>. Batteries may be safely stored in two methods:

   a. All batteries can be stored in holders on the charging circuit as long as they are physically disconnected from any energy source and test loads using the physical kill switches.

   b. Batteries can be safely stored in their plastic shipping containers.

   c. Batteries can be safely stored on their wooden holders, those provided by the Railgun laboratory or those created by the Power laboratory, as long as these holders are physically separated from BMS. The physical separation will prevent accidental discharges around the BMS in case they are knocked over.

THIS PAGE INTENTIONALLY LEFT BLANK

APPENDIX B. BMS CHARGING MODEL AND MATLAB® CODE

This appendix includes the entire model of the BMS charging model and the simulations associated MATLAB® code. The model figures show first the entire model and then drill down into the various subsystems.

Figure 34 shows the overview of the BMS charging model.

Battery Energy Storage System (BESS)

Created by: Maj Frank Filler with significant assistance from Proj Julian and Prof Oriti.
Parts of this simulation are copied directly from labs from their classes.
Start Date: 090714   Last Updated: 091125
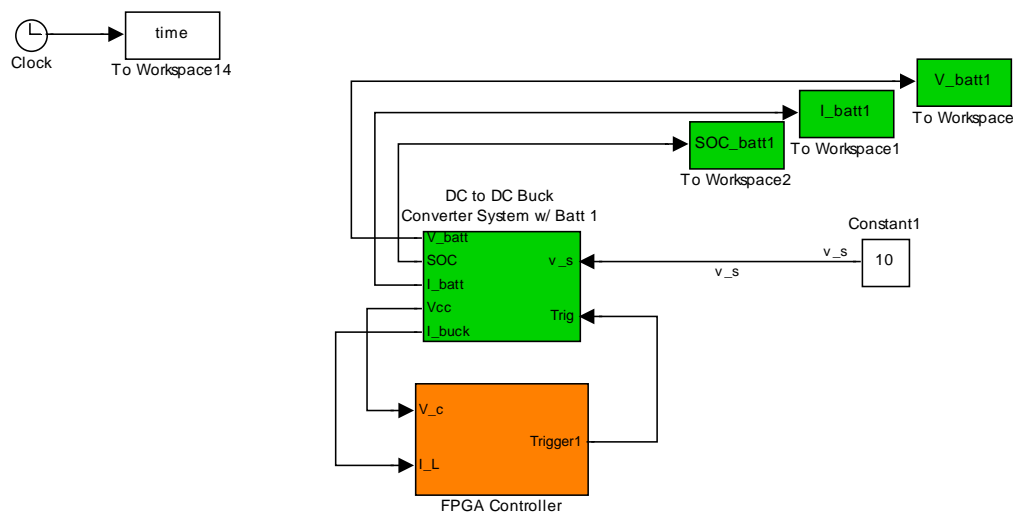
Figure 34.   BMS Charging Model Overview.

Figure 35 shows the model of the FPGA controller.

Figure 35.   FPGA Controller Model.

Figure 36 shows the models of the buck converter and battery.

Figure 36.   Buck Converter and Battery Models.

Figure 37 shows the battery model parameter calculations.
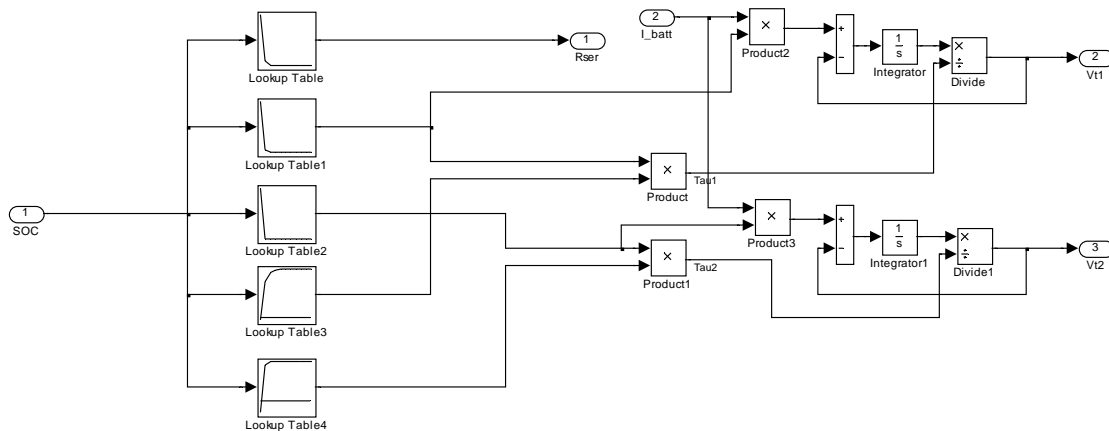
Figure 37.   Battery Model Parameter Calculations.

The following MATLAB® code provides the initial conditions for the execution of the BMS charging model.

```
%BESS.m
%
%This code completes the necessary steps to complete the thesis research
%for the Battery Energy Storage System (BESS) for the Navy's Railgun.
%This work was completed by Maj Frank Filler with substantial guidance and
%direction Dr. Alexander Julian.
%
%Maj Frank Filler        Date Started:   26 Jan 09
%                        Date Updated:   25 Nov 09


%%%%%%%%%%%%%%%%%%%%%%%%%%%%%%%%%%%%%%%%%%%%%%%%%%%%%%%%%%%%%%%%%%%%%%%%%
%Defined variables.
%%%%%%%%%%%%%%%%%%%%%%%%%%%%%%%%%%%%%%%%%%%%%%%%%%%%%%%%%%%%%%%%%%%%%%%%%
tstep=1e-4;
Vs_peak=120*sqrt(2);     %Peak voltage of the energy voltage.
fs=60;                   %Frequency of the energy voltage.
f_conv=10e3;             %Max Sampling Frequency of the voltage to
```

67

```
                        %frequency converter.   Used in the simulation to
                        %slow reaction of the controller.
ws=2*pi*fs;

tout_calc=0:tstep:tstop;

ST_freq=30e3;           %Slope of the ramp for PWM.

N1=1;

N2=10;

N=N1/N2;                %Transformer turns ratio.

%PI gains for the current and voltage controllers.

Kp_i=3*.5;

Ki_i=3.8*.5;

Kp_v=2*.7;

KI_v=6*.5;

Cf=4.4e-3;              %Filter capacitor.

R_bl=2000;             %Bleed resistor.

L=66.0e-6;             %Inductor in the buck converter.

Cc=100e-6;            %Capacitor in the buck converter.

Rl=0;                 %Resistance of the buck inductor.

Ls=0;                 %Line inductance.

Lsbatt=2e-3;          %Inductance necessary in the battery model.

Rls=1e-3;             %Resistance of the line inductance.

diode_loss=1.4;       %Simulates the volt. loss in the diode rectifier.

SOC_lu1=0:.1:1.00;    %SOC values for the model parameters lookup tables.

sample_delay=10000;   %Delays the end of charge detector.

batt_type=4;          %Choose 1 for A123 32113, 2 for A123 26650, 3
                      %for Saft VL-12v, or 4 for the test model battery.


%Variables necessary from Prof Oriti's diode rectifier model.

ampl=Vs_peak;

delta=25e-7;          %Delay time.

Cdc=Cf;


%%%%%%%%%%%%%%%%%%%%%%%%%%%%%%%%%%%%%%%%%%%%%%%%%%%%%%%%%%%%%%%%%%%%%%%
```

```matlab
%Define type of battery.  Each battery will have a Voc vs. SOC values for a
%lookup table-NOTE-these values are discharge current and temperature
%dependent!
%%%%%%%%%%%%%%%%%%%%%%%%%%%%%%%%%%%%%%%%%%%%%%%%%%%%%%%%%%%%%%%%%%%%%%%%%%

if batt_type==1;


    CC_I=10;
    CV_V=3.6;
    CV_cutoff=0.4;
    Discharge_cutoff=2.5;
    Capacity=4.4;
    Load=1;                    %Load for the BESS discharge (20 A).
else if batt_type==2;


        CC_I=3;                %Can go to 10 Amps for "fast charging."
        CV_V=3.6;
        CV_cutoff=0.2;
        Discharge_cutoff=2.5;
        Capacity=2.3;
        Load=1;                %Load for the BESS discharge (20A).
    else if batt_type==3;


            CC_I=10;           %Can go to 12 Amps.
            CV_V=4.1;
            CV_cutoff=0.1;
            Discharge_cutoff=2.5;
            Capacity=12;
            Load=1;            %Load for the BESS discharge (20 A).
        else
            CC_I=0.8;          %This is the battery modeled in the paper.
            CV_V=4.1;
            CV_cutoff=0.01;
```

69

```
            Discharge_cutoff=3;

            Capacity=0.850;

            Load=6.40;            %Load for the BESS discharge.  Creates a
                                  %640 mA discharge (using nominal voltage).

            Voc_lu=[3; 3.68; 3.71; 3.76; 3.79; 3.8; 3.83; 3.87; 3.95; ...
                4; 4.1];

            SOC_lu=[0; .10; .20; .30; .40; .50; .60; .70; .80; .90; 1.00];

            Rser=0.1562*exp(-24.37.*SOC_lu1)+0.07446;

            Rt1=0.3208*exp(-29.14.*SOC_lu1)+0.04669;

            Rt2=6.603*exp(-155.2.*SOC_lu1)+0.04984;

            Ct1=-752.9*exp(-13.51.*SOC_lu1)+703.6;

            Ct2=-6056*exp(-27.12.*SOC_lu1)+4475;

        end %else if batt_type==3;

      end %else if batt_type==2;

  end %if batt_type==1;


  %%%%%%%%%%%%%%%%%%%%%%%%%%%%%%%%%%%%%%%%%%%%%%%%%%%%%%%%%%%%%%%%%%%
  %Chen-Rincon-Mora battery model.
  %%%%%%%%%%%%%%%%%%%%%%%%%%%%%%%%%%%%%%%%%%%%%%%%%%%%%%%%%%%%%%%%%%%


  f1=1;              %Cycle number correction factor.
  f2=1;              %Temperature dependent correction factor.
  Rsd=1e9;           %Self-discharge resistance.
  Ccap=3600*Capacity*f1*f2;     %Capacity capacitance-would need to be
                                %dynamically calculated to take temperature
                                %into account.
```

The following MATLAB® code repeatedly runs the simulation in order to collect runtime data throughout the charging process.

```
%BESS_Start.m
%
%This code completes the necessary steps to complete the thesis research
%for the Battery Energy Storage System (BESS) for the Navy's Railgun.
```

70

```matlab
%This work was completed by Maj Frank Filler with substantial guidance and
%direction Dr. Alexander Julian.   VOC_initial and tstop must be set in this
%m file before running simulation.   All other variables are set in Bess.m.
%
%Maj Frank Filler        Date Started:   24 Aug 09
%                        Date Updated:   25 Nov 09


%%%%%%%%%%%%%%%%%%%%%%%%%%%%%%%%%%%%%%%%%%%%%%%%%%%%%%%%%%%%%%%%%%%%%%%%%%
%Initial formatting.
%%%%%%%%%%%%%%%%%%%%%%%%%%%%%%%%%%%%%%%%%%%%%%%%%%%%%%%%%%%%%%%%%%%%%%%%
clear all
close all
format compact
home


%%%%%%%%%%%%%%%%%%%%%%%%%%%%%%%%%%%%%%%%%%%%%%%%%%%%%%%%%%%%%%%%%%%%%%%%%%
%Run Simulation at various SOCs.   VOC_initial must be set in this m file
%before running simulation.   All other variables are identified in Bess.m.
%%%%%%%%%%%%%%%%%%%%%%%%%%%%%%%%%%%%%%%%%%%%%%%%%%%%%%%%%%%%%%%%%%%%%%%%%
VOC_initial=0;          %Initial SOC for the batteries.   Use 99.73% to test
                       %for end of charge detection. Use 99.99% to test
                       %for firing sequence.
tstop=20;
sim('BESS_Simulation_v3_01')
fac=0.1;
n=fac*length(time);

figure(1)
subplot(3,1,1)
plot(time, I_batt1)
title('Battery 1 Current Curve')
ylabel('Current (amperes)')
```

```
xlabel('Time (seconds)')

axis([0 tstop 0 (CV_V+.5)])

grid on

subplot(3,1,2)

plot(time, V_batt1)

title('Battery 1 Voltage Curve')

ylabel('Voltage (volts)')

xlabel('Time (seconds)')

grid on

subplot(3,1,3)

plot(time, 100.*SOC_batt1)

title('Battery1 SOC')

ylabel('SOC (%)')

xlabel('Time (seconds)')

grid on


%Plot more specifics of the controller.

figure(111)

subplot(5,1,1)

plot(time, V_error)

ylabel('V error')

grid on

subplot(5,1,2)

plot(time, I_ref)

ylabel('I ref')

grid on

subplot(5,1,3)

plot(time, I_error)

ylabel('I error')

grid on

subplot(5,1,4)

plot(time, Duty)

ylabel('Duty Cycle')
```

```matlab
grid on
subplot(5,1,5)
plot(time, V_batt1)
ylabel('Battery Voltage')
grid on

%Begin the averaging for the final plot.
I_batt1(1:n,:)=[];
V_batt1(1:n,:)=[];
SOC_batt1(1:n)=[];
I_batt1_final=mean(I_batt1);
V_batt1_final=mean(V_batt1);
SOC_batt1_final=mean(SOC_batt1);

%pause

fac=0.5;
n=fac*length(time);

for ii=.01:.02:.99
VOC_initial=ii;
tstop=20;
sim('BESS_Simulation_v3_01')

figure(int8(ii*100))
subplot(3,1,1)
plot(time, I_batt1)
title('Battery 1 Current Curve')
ylabel('Current (amperes)')
xlabel('Time (seconds)')
axis([0 tstop 0 (CV_V+.5)])
grid on
subplot(3,1,2)
```

```matlab
plot(time, V_batt1)
title('Battery 1 Voltage Curve')
ylabel('Voltage (volts)')
xlabel('Time (seconds)')
grid on
subplot(3,1,3)
plot(time, 100.*SOC_batt1)
title('Battery1 SOC')
ylabel('SOC (%)')
xlabel('Time (seconds)')
grid on


%Plot more specifics of the controller.
figure(111)
subplot(5,1,1)
plot(time, V_error)
ylabel('V error')
grid on
subplot(5,1,2)
plot(time, I_ref)
ylabel('I ref')
grid on
subplot(5,1,3)
plot(time, I_error)
ylabel('I error')
grid on
subplot(5,1,4)
plot(time, Duty)
ylabel('Duty Cycle')
grid on
subplot(5,1,5)
plot(time, V_batt1)
ylabel('Battery Voltage')
```

```matlab
grid on

I_batt1(1:n,:)=[];

V_batt1(1:n,:)=[];

time(1:n)=[];

SOC_batt1(1:n)=[];

I_batt1_final=[I_batt1_final; mean(I_batt1)];

V_batt1_final=[V_batt1_final; mean(V_batt1)];

SOC_batt1_final=[SOC_batt1_final; mean(SOC_batt1)];


end %ii=???


%Discharge period.
VOC_initial=.999;
tstop=20;
sim('BESS_Simulation_v3_01')


figure(100)
subplot(2,1,1)
plot(time, I_batt1, time, V_batt1)
title('Battery 1 I-V Curve')
ylabel('Current (amperes)/Voltage (volts)')
xlabel('Time (seconds)')
legend('Current','Voltage')
axis([0 tstop 0 (CV_V+.5)])
grid on
subplot(2,1,2)
plot(time, 100.*SOC_batt1)
title('Battery1 SOC')
ylabel('SOC (%)')
xlabel('Time (seconds)')
grid on
```

75

```
I_batt1(1:n,:)=[];

V_batt1(1:n,:)=[];

time(1:n)=[];

SOC_batt1(1:n)=[];

I_batt1_final=[I_batt1_final; mean(I_batt1)];

V_batt1_final=[V_batt1_final; mean(V_batt1)];

SOC_batt1_final=[SOC_batt1_final; mean(SOC_batt1)];


%%%%%%%%%%%%%%%%%%%%%%%%%%%%%%%%%%%%%%%%%%%%%%%%%%%%%%%%%%%%%%%%%%%%%%%%%%
%Plot overall data.
%%%%%%%%%%%%%%%%%%%%%%%%%%%%%%%%%%%%%%%%%%%%%%%%%%%%%%%%%%%%%%%%%%%%%%%%%%


figure(1000)

plot(100.*SOC_batt1_final, I_batt1_final, 'r*--', 100.*SOC_batt1_final,
V_batt1_final,'b*--')

title('Charge Profile')

ylabel('Current (amperes)/Voltage (volts)')

xlabel('SOC (%)')

legend('Current','Voltage', 'location', 'east')

grid on
```

LIST OF REFERENCES

[1]   Electricity Storage Association, "Installed Systems as of November 2008," http://electricitystorage.org/pix/ES-0023-System-Ratings7.gif, last visited 9 November 2009.

[2]   J. A. McDowall, "Status and Outlook of the Energy Storage Market Power," *Engineering Society General Meeting, 2007*. IEEE, 24–28 June 2007, pp. 1–3.

[3]   Electricity Storage Association, "Output Energy Density," http://electricitystorage.org/pix/photo_EnergyDensity.gif, last visited 9 November 2009.

[4]   Yuang-Shung Lee and Ming-Wang Cheng, "Intelligent Control Battery Equalization for Series Connected Lithium-Ion Battery Strings," *Industrial Electronics*, IEEE Transactions, Volume 52, Issue 5, October 2005, pp. 1297–1307.

[5]   A. M. Rahimi, "A Lithium-Ion Battery Charger for Charging up to Eight Cells," in *Vehicle Power and Propulsion,* IEEE Conference, 2005, pp 6–8.

[6]   V. L., Teofilo, L. V. Merritt, and R. P. Hollandsworth, "Advanced Lithium Ion Battery Charger," *Aerospace and Electronic Systems Magazine, IEEE*, Volume 12, Issue 11, November 1997, pp. 30–36.

[7]   Chia-Hsiang Lin, Chi-Lin Chen, Yu-Huei Lee, Shih-Jung Wang, Chun-Yu Hsieh, Hong-Wei Huang, and Ke-Horng Chen, "Fast Charging Technique for Li-Ion Battery Charger," *Electronics, Circuits, and Systems, 2008*, ICECS 2008. 15th IEEE International Conference, 31 August – 3 September 2008, pp. 618–621.

[8]   Yi-Hwa Liu and Jen-Hao Teng, "Design and Implementation of a Fully-digital Lithium-Ion Battery Charger," TENCON 2006, 2006 IEEE Region 10 Conference, 14-17 November 2006, pp. 1–4.

[9]   Yi-Hwa Liu, Jen-Chung Li, and Jen-Hao Teng, An FPGA-Based Lithium-Ion Battery Charger System," TENCON 2004. 2004 IEEE Region 10 Conference, 21–24 November 2004, Vol. 4, pp. 435–438.

[10]   Panasonic, Lithium Ion Batteries: Individual Data Sheet, CGA103450A, January 2007.

[11]   Ming Tang and Stuart T, "Selective Buck-Boost Equalizer for Series Battery Packs," *Aerospace and Electronic Systems*, IEEE Transactions, Volume 36, Issue 1, January 2000, pp. 201–211.

[12]   Chol-Ho Kim, Hong-Sun Park, Chong-Eun Kim, Gun-Woo Moon, Joong-Hui Lee, and Jeon Keun Oh, "Charge Equalization Converter with Parallel Primary Winding for Series Connected Lithium-Ion Battery Strings in HEV," *Power Electronics*, 2007, ICPE '07, 7th International Conference on Power Electronics, 22–26 October 2007 pp. 795–800.

[13]   Donald Schelle and Jorge Castorena, "Buck-Converter Design Demystified," *Power Electronics Technology*, June 2006, pp. 46–53.

[14]   Jerrold Foutz, "Switching-Mode Power Supply Design Tutorial Simple Switching Topologies," http://www.smpstech.com/tutorial/t03top.htm, last visited 22 November 2009.

[15]   Maxim Integrated Products, Application Note 2031, http://www.smpstech.com/tutorial/t03top.htm, last visited 22 November 2009.

[16]   Ned Mohan, Tore M. Undeland, and William P. Robbins, *Power Electronics*, 3rd Edition, John Wiley and Sons, Inc, New Jersey, 2003.

[17]   SGS-Thomson Microelectronics, Application Note 253/1088, pp. 1–6.

[18]   Abraham I. Pressman, *Switching Power Supply Design*, 2nd Edition, McGraw-Hill, New York, 1998.

[19]   G. Oriti, "Buck Low Pass Filter Analysis," class notes for EC3150, Electrical and Computer Department, Naval Postgraduate School, Fall 2008.

[20]   Linear Technology Corporation, LT3010/LT3010-5 Micropower Linear Regulator Data Sheet, pp. 1–16.

[21]   National Semiconductor, LM231A/LM231/LM331A/LM331 Precision Voltage-to-Frequency converters Data Sheet, pp. 1–15.

[22]   LEM, Current Transducer HMS 5 -20-P Data Sheet, pp. 1–6.

[23]   James W. Nilsson and Susan A. Riedel, *Electronic Circuits*, 8th Edition, Pearson Prentice Hall, New Jersey, 2008.

[24]   Wikipedia, "Galvanic Isolation," http://en.wikipedia.org/wiki/Galvanic_isolation, last visited 24 November 2009.

[25]   Ametherm, MS 35 3R030 Data Sheet.

[26]   Signal Transformer, Two-4-One Power Transformers Data Sheet, pp. 1–2.

[27]   National Semiconductor Corporation, LM35 Precision Centigrade Temperature Sensors Data Sheet, November 2000, pp. 1–13.

[28]   Wikipedia, "Pulse-width Modulation," http://en.wikipedia.org/wiki/Pulse-width_modulation, last visited 25 November 2009.

[29]   Min Chen and Gabriel A. Rincon-Mora, "Accurate Electrical Battery Model Capable of Predicting Runtime and I-V Performance," IEEE Transactions on Energy Conversion, volume 21, pp. 504–511, June 2006.

[30]   Bernhard Schweighofer, Klaus M. Raab, and Georg Brasseur, "Modeling of High Power Automotive Batteries by the Use of an Automated Test System," IEEE Transactions on Instrumentation and Measurement, volume 52, pp. 1087–1091, August 2003.

[31]   ST Microelectronics, STS14N3LLH5 STripFET V Power MOSFET Data Sheet, pp. 1–12.

[32]   Crydom, Inc., D06D Series Data Sheet, pp. 1–4.

[33]   Microchip Technology, Inc., MCP616/7/8/9 Mircropower Bi-CMOS Op Amps Data Sheet, pp. 1–38.

[34]   A123 Systems, Inc., 32113 Specifications Data Sheet.

[35]   A123 Systems, Inc., High Power Lithium Ion ANR26650M1 Data Sheet.

[36]   Saft America, Inc., Rechargeable lithium-ion battery VL12 V Data Sheet, pp. 1–2.

[37]   Roy D. Merrill, "Engineering Safety Note, Solid-State Heat-Capacity-Laser (SSHCL) Lithium-Ion Battery System," Lawrence Livermore National Laboratory, 26 March 2003.

THIS PAGE INTENTIONALLY LEFT BLANK

INITIAL DISTRIBUTION LIST

1. Defense Technical Information Center
    Ft. Belvoir, Virginia

2. Dudley Knox Library
    Naval Postgraduate School
    Monterey, California

3. Dr. Jeffrey Knorr
    Electrical Engineering and Computer Department
    Code EC/Ko
    Naval Postgraduate School
    Monterey, California

4. Dr. Alexander Julian
    Electrical Engineering and Computer Department
    Code EC/J1
    Naval Postgraduate School
    Monterey, California

5. Dr. Roberto Cristi
    Electrical Engineering and Computer Department
    Code EC/C1
    Naval Postgraduate School
    Monterey, California

6. Marine Corps Representative
    Naval Postgraduate School
    Monterey, California

7. Director, Training and Education, MCCDC, Code C46
    Quantico, Virginia

8. Director, Marine Corps Research Center, MCCDC, Code C40RC
    Quantico, Virginia

9. Marine Corps Tactical Systems Support Activity
    (Attn: Operations Officer)
    Camp Pendleton, California

10. Jack Bernardes, CIV NSWCDD, Q20
    Naval Surface Warfare Center

11. Steve B. Swindler, PE Electrical Engineer
    Naval Surface Warfare Center
    Carderock Division Code 9820